Petroleum Science 20 (2023) 2709–2725

Contents lists available at ScienceDirect

Petroleum Science

journal homepage: www.keaipublishing.com/en/journals/petroleum-science

Original Paper

Maceral evolution of lacustrine shale and its effects on the development of organic pores during low mature to high mature stage: A case study from the Qingshankou Formation in northern Songliao Basin, northeast China

Liu Wang [a, b], Bo Liu [a, b, *], Long-Hui Bai [a, b], Mehdi Ostadhassan [a, b], Thomas Gentzis [c], Bo-Yang Wang [a, b], Yi-Zhang Wang [d]

[a] Key Laboratory of Continental Shale Hydrocarbon Accumulation and Efficient Development, Ministry of Education, Northeast Petroleum University, Daqing, Heilongjiang, 163318, China
[b] Accumulation and Development of Unconventional Oil and Gas, State Key Laboratory Cultivation Base, Northeast Petroleum University, Daqing, Heilongjiang, 163318, China
[c] Core Laboratories, Reservoir Geology Group, 6316 Windfern Road, Houston, TX, 77040, USA
[d] Exploration and Development Research Institute of Daqing Oilfield Co Ltd, Daqing, Heilongjiang, 163712, China

ARTICLE INFO

Article history:
Received 4 October 2022
Received in revised form
9 April 2023
Accepted 21 August 2023
Available online 23 August 2023

Edited by Jie Hao and Teng Zhu

Keywords:
Lacustrine shale
Maceral evolution
Organic pores
Scanning electron microscopy
Reflected light microscopy

ABSTRACT

Organic matter (OM) hosted pores are crucial for the storage and migration of petroleum in shale reservoirs. Thermal maturity and macerals type are important factors controlling the development of pores therein. In this study, six lacustrine shale samples with different thermal maturities from the first member of the Qingshankou Formation in the Songliao Basin, of which vitrinite reflectance (R_o) ranging from 0.58% to 1.43%, were selected for a comparative analysis. Scanning electron microscopy (SEM) and reflected light microscopy were combined to investigate the development of organic pores in different macerals during thermal maturation. The results show that alginite and liptodetrinite are the dominant primary macerals, followed by bituminite. Only a few primary organic pores developed in the alginite at the lowest maturity (R_o = 0.58%). As a result of petroleum generation, oil-prone macerals began to transform to initial-oil solid bitumen at the early oil window (R_o = 0.73%) and shrinkage cracks were observed. Initial-oil solid bitumen cracked to oil, gas and post-oil bitumen by primary cracking (R_o = 0.98%). Moreover, solid bitumen (SB) was found to be the dominant OM when R_o > 0.98%, which indicates that SB is the product of oil-prone macerals transformation. Many secondary bubble pores were observed on SB, which formed by gas release, while devolatilization cracks developed on migrated SB. Additionally, at the late oil window (R_o = 1.16%), migrated SB filled the interparticle pore spaces. With further increase in temperature, the liquid oil underwent secondary cracking into pyrobitumen and gas, and spongy pores developed on the pyrobitumen at higher levels of maturity (R_o = 1.43%), which formed when pyrobitumen cracked into gas. Vitrinite and inertinite are stable without any visible pores over the range of maturities, verifying their low petroleum generation potential. In addition, it was concluded that clay minerals could have a catalytic effect on the petroleum generation, which may explain why organic-clay mixtures had more abundant pores than single OM particles. However, after R_o > 0.98%, authigenic minerals occupied the organic pore spaces on the organic-clay mixtures, resulting in fewer pores compared to those observed in samples at the early to peak oil window.

1. Introduction

In recent years, shale oil and gas have become important resources for petroleum exploration and development (Jarvie, 2012; Liu et al., 2012; Curiale and Curtis, 2016). And CO_2 storage in shale

* Corresponding author. Key Laboratory of Continental Shale Hydrocarbon Accumulation and Efficient Development, Ministry of Education, Northeast Petroleum University, Daqing, Heilongjiang, 163318, China.
E-mail address: liubo@nepu.edu.cn (B. Liu).

https://doi.org/10.1016/j.petsci.2023.08.025

reservoirs is also of growing interest to slow down the processes of climate change (Merey and Sinayuc, 2016). The interconnected organic pore network is an important controlling of the reservoir storage space and permeability in shale formations (Slatt and O'Brien, 2011; Loucks et al., 2012; Liu et al., 2018; Ko et al., 2018). The complexity and extent of the organic pore space is dependent on the organic matter (OM) types, thermal maturity, mineral composition and total organic carbon (TOC) content (Curtis et al., 2012; Mastalerz et al., 2013; Pommer and Milliken, 2015; Furmann et al., 2016; Ko et al., 2016; Knapp et al., 2020). Therefore, evaluating OM transformation and its associated organic pores during thermal evolution stage play a key role in shale reservoir characterization.

The type or the origin of OM is an important controlling factor in pore development. Curtis et al. (2012) reported that pores that are developed adjacent to OM particles in the same sample could have significant differences in their abundance, which is due to the different types of OM follow specific evolutionary pathways during thermal maturation. When OM is exposed to heat and pressure during burial, its thermal maturity will progress and the oil-prone macerals (bituminite, alginite and liptodetrinite) will be transformed into secondary macerals-such as solid bitumen (SB) (Wood et al., 2015; Misch et al., 2019). Vitrinite, inertinite and zooclasts basically do not transform during thermal maturation because of their low hydrocarbon generation potential (Misch et al., 2019). The maceral types and abundance of the dominant components vary under different sedimentary environments and thermal maturation (Liu et al., 2019a). Lamalginite is the most abundant primary maceral while terrigenous OM is minor in the Songliao Basin lacustrine shale samples (Zhang et al., 2021; Liu et al., 2022b). Alginite derived from Tasmanites cysts and bituminite is the primary oil-prone macerals in the New Albany marine shale samples (Liu et al., 2017a).

OM-hosted pores in black shales were normally divided into primary and secondary organic pores (Pommer and Milliken, 2015; Knapp et al., 2020). Primary organic pores are inherited from the original organic material such as immature structured and amorphous OM (Löhr et al., 2015). However, primary organic pores appear to be less abundant in samples due to mechanical compaction (Dong et al., 2017). Secondary organic pores are hosted by SB or pyrobitumen (Liu et al., 2017a), while its shape and size are easily affected by the degree of thermal maturity. Among them, bubble pores are mostly developed in the oil window, and sponge pores are mostly developed in the higher maturity stages (Reed et al., 2020). Liu et al. (2022b) concluded that organic pores are poorly developed in the immature-low maturity and early oil stage while increasing greatly from peak oil maturity stage to late oil maturity stage in the Songliao Basin. Nonetheless, all their studies are not associated with organic pore evolution model of different macerals. The organic pore network is also affected by the surrounding inorganic minerals. The catalysis effect of clay minerals can alter the temperature at which organic pores are formed and makes it more complicated, so it does not follow general thermal maturity rule (Lao et al., 1989). Meanwhile, some studies have also shown that clay minerals can have a certain inhibitory effect on petroleum generation (Liu et al., 2018).

Furthermore, to study nanometer-scale OM-hosted pores in shales, scanning electron microscope (SEM) is the most used method. However, OM appears black in SEM images, which somehow makes it difficult to distinguish maceral types using SEM (Liu et al., 2022a) while optical microscopey can be used for this purpose. Meanwhile, optical microscopes are limited in their magnification, so that SEM-visible organic pores cannot be recognized. Thus, correlative microscopy would be necessary to overcome these issues which are done in a limited scope solely for the goal of assessing organic pore. Teng et al. (2022) combined SEM and optical microscopy to study OM types and their control on the development of organic pores in overmature shale samples from the Longmaxi Formation in the Sichuan Basin of China. They found that organic pores mainly exist in pyrobitumen in the overmature stage. Liu et al. (2017a) combined SEM and reflected light microscope to study the changes in organic pores in different types of OM in shale samples from the New Albany Formation (USA) ranging from early maturity to the gas window and found that primary organic pores are mainly developed in inertinite, while secondary organic pores are abundant in SB.

The Songliao Basin is one of the largest continental basins all over the world (total area is about 260,000 km^2), in which the Upper Cretaceous Qingshankou shale is the most prolific source rock (Bechtel et al., 2012; Bai et al., 2022; Zhou et al., 2022; Liu et al., 2023a). The majority of the previous studies of maceral evolution and its effects on the development of organic pores mostly were carried out on marine shales, while only a few studies on lacustrine ones without correlative microscopy in the oil generation window were performed (Zhang et al., 2021; Liu et al., 2022a, 2023b). Therefore, in this study, we combined SEM and optical microscopy to investigate the development of organic pores in different macerals in six lacustrine shale samples ranging from low to high thermal maturity from the Qingshankou Formation in the Songliao Basin. The main objectives are to analyze the evolution of macerals and to observe the development of organic pores in different macerals during thermal maturation.

2. Samples and methods

2.1. Samples

The Songliao Basin is a large Mesozoic-Cenozoic continental petroliferous basin located in the northeast of China (Liu et al., 2019c, 2023a; Wang B. et al., 2022). It has six first-order structural units, and the central depression is the main hydrocarbon distribution area (Fig. 1a-b). The Qingshankou Formation was deposited in a large lake influenced by periodic marine incursion period, and the maximum area of the basin is about 8.7×10^4 km^2 (Fig. 1d) (Liu et al., 1993, 2023a; Huang et al., 2013). The basin is formed in a warm and humid paleoclimate, favorable for the occurrence of deep to semi-deep lakes with anoxic reducing bottom water environments conducive to the preservation and enrichment of OM (Liu et al., 2019c). The formation contains a set of dark organic-rich shales with a thickness of approximately 100 m. The TOC contents are between 2.0 w.t.% and 8.7 w.t.% and the kerogen type is mainly type I and type II. Thermal maturity (vitrinite reflectance, R_o) of the formation ranges between 0.5% and 1.6% to ultimately make this formation an excellent shale play target (Bai et al., 2021; Liu et al., 2021).

In this study, six organic rich dark shale core samples with different depth were selected (Fig. 1c) to determine the existing macerals and assess the evolution of organic pores at different thermal maturity levels. Each sample was homogenized into several aliquots for different analysis, including TOC analysis, rock pyrolysis (Rock-Eval), reflected light microscope and SEM observation.

2.2. Methods

2.2.1. TOC and Rock-Eval pyrolysis

The TOC was measured using an Eltra Helios CS elemental analyzer on samples pre-treated with hydrochloric acid to remove carbonates (Liu et al., 2017b). The standard procedures of Rock-Eval pyrolysis was performed following Liu et al. (2019c) and

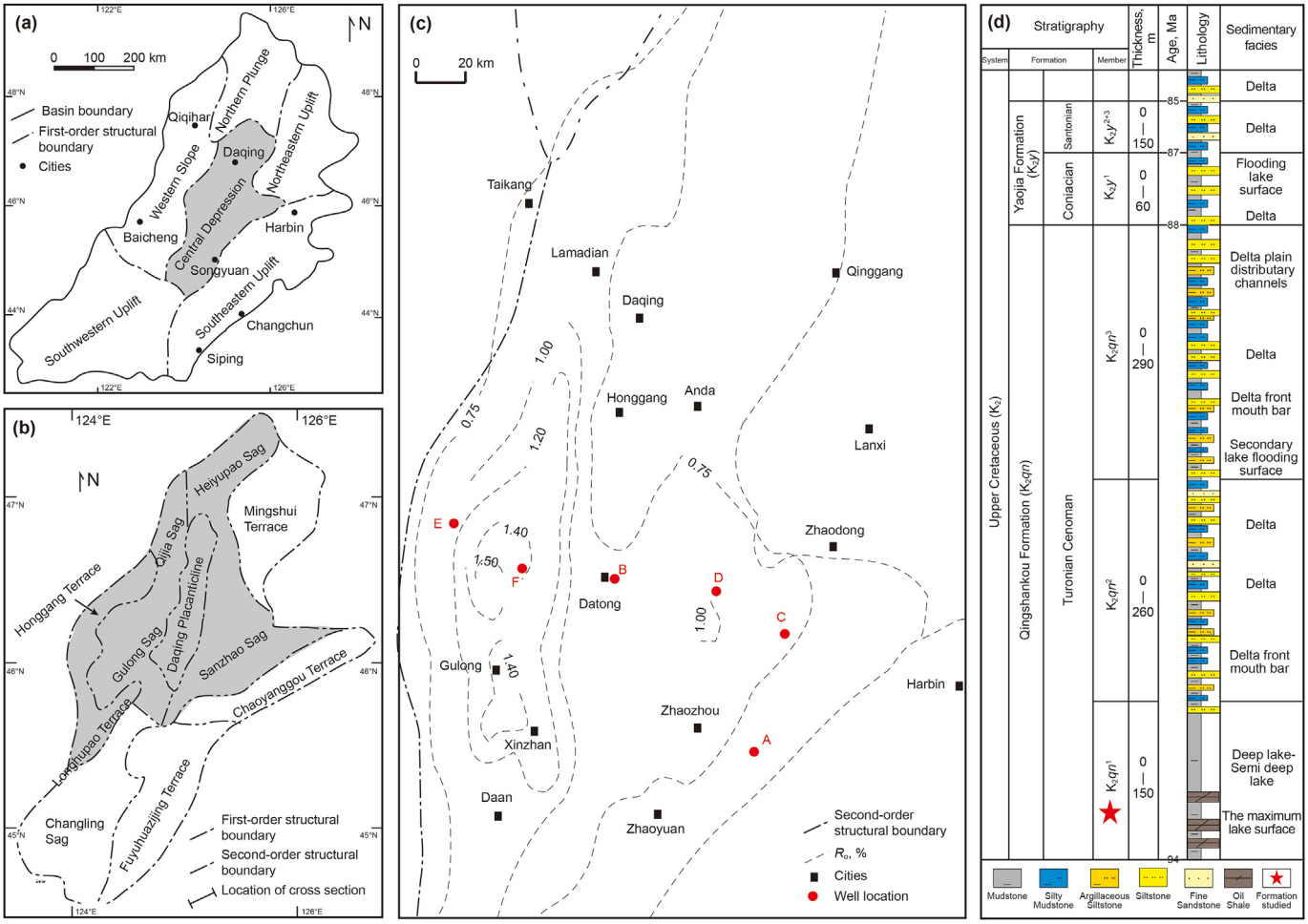

Fig. 1. Map showing the location of the Songliao Basin. (a) Study area (Central depression) (b) the location of the sampling sites (c) General lithologic stratigraphy of the Songliao Basin (d) (modified from Liu et al., 2019c).

geochemical parameters including S_1, S_2, S_3, T_{max}, Hydrogen Index (HI = 100 × S_2/TOC) were obtained accordingly. S_1 represents the free hydrocarbon in the sample, S_2 represents the pyrolysis yield and is an indicator of the remaining generation potential, and S_1+S_2 represents the total hydrocarbon potential (Jarvie, 2012). T_{max} is the temperature at the maximum of the S_2 peak and can be used to evaluate thermal maturity (Langford and Blanc-Valleron, 1990).

2.2.2. Reflected light microscope

The maceral classification and terminology applied in this study are based on the International Committee for Coal Petrology (ICCP) System (vitrinite classification, ICCP, 1998; inertinite classification, ICCP, 2001; liptinite classification, Pickel et al., 2017). Maceral types were identified using optical microscopy in reflected light and fluorescence modes (Taylor et al., 1998). Whole-rock pellets were cut from the samples perpendicular to the bedding planes and polished, and analyzed with a Leica DM-RXP + Q550IW microscope using both reflected light and oil immersion. 20 × and 50 × objectives were used with white light and fluorescence, respectively, to observe the reflected light color, intensity and structural morphology of the macerals and SB. The random R_o of six shale samples were measured under a Zeiss axio image Z1 multi-functional microscope following ASTM (2014).

2.2.3. SEM

The six shale samples were analyzed by a Zeiss Sigma SEM coupled with an Oxford X-Max 50 N energy-dispersive X-ray spectroscopy (EDS) detector. Blocks of 1 × 1 cm^2 and 0.5 cm in height were cut perpendicular to the bedding direction from the shale samples. After mechanical polishing, argon ion mill was performed on the surface using an America Gatan 697C ion polisher, which removed the artificial pits generated during the mechanical polishing process. The working voltage of the argon ion polisher was 6 kV and the grinding time was 1.5 h. The SEM work was carried out in the vacuum mode with the accelerating voltage of 10–20 keV and 20 nA.

To identify and examine the macerals using SEM the following procedure was used: first, a general knowledge of thermal maturity and original OM composition of the samples is obtained (Liu et al., 2019b, 2022a). Then, at low magnifications (100–2000 ×) in back-scattered electron (BSE) mode, the primary macerals and SB were identified based on the shape and size of the OM particles and their contact correlation with the surrounding minerals. Subsequently, at higher magnifications (2000–15000 ×), the maceral types were confirmed and their morphology and pore development were observed. To avoid the electric charge effect, the shale samples were fixed on the sample holder with conductive glue and coated with 13 nm gold to enhance the conductivity. Additionally, a high-resolution energy spectrum detector was used for elemental analysis of inorganic minerals while the concentration of carbon element can confirm the presence of OM. The working voltage of the energy dispersive ray was 10 kV, and the total time was more

than 20,000 s. This provided us with elemental maps from the surface to evaluate mineral phases accompanying the OM.

3. Results

3.1. Bulk geochemical parameters

The bulk geochemical parameters of the six samples are listed in Table 1. The TOC values vary from 3.26 w.t.% to 5.13 w.t.%. The values of S_1 vary from 1 mg/g to 4.97 mg/g, and the values of S_2 vary from 7.38 mg/g to 31.25 mg/g. Moreover, hydrocarbon potential (S_1+S_2) of the samples was calculated from 10.93 mg/g to 36.49 mg/g. Thermal maturity of the sample, R_o was measured to change from 0.58% to 1.43% indicating a wide range of thermal maturities. According to Liu et al. (2022b)'s division of hydrocarbon generating evolution stage of the Qingshankou Formation shale, the samples can be assigned to five maturity categories. Sample A (R_o = 0.58%) and B (R_o = 0.69%) are at low mature stage (R_o < 0.7%), the mature stage (R_o = 0.7%–1.4%) can be further sub-divided into three substages: early oil maturity (R_o = 0.7%–0.85%), peak oil maturity (R_o = 0.85%–1.1%), and late oil maturity (R_o = 1.1%–1.4%). Sample C (R_o = 0.73%) is at early oil mature stage, sample D (R_o = 0.98%) is at peak oil mature stage, sample E (R_o = 1.16%) is at late oil mature stage and finally sample F (R_o = 1.43%) is at high mature stage (R_o = 1.4%–2.0%). The HI values were measured to vary from 206 mg/g to 775 mg/g. The T_{max} values were measured from 449 °C to 460 °C, also confirming a wide maturity range of the samples from almost immature to the end of the wet gas window as was found from the R_o result. The cross-plot of T_{max} versus HI (Fig. 2) shows that the OM of the Qingshankou Formation shale is dominated by type I kerogen.

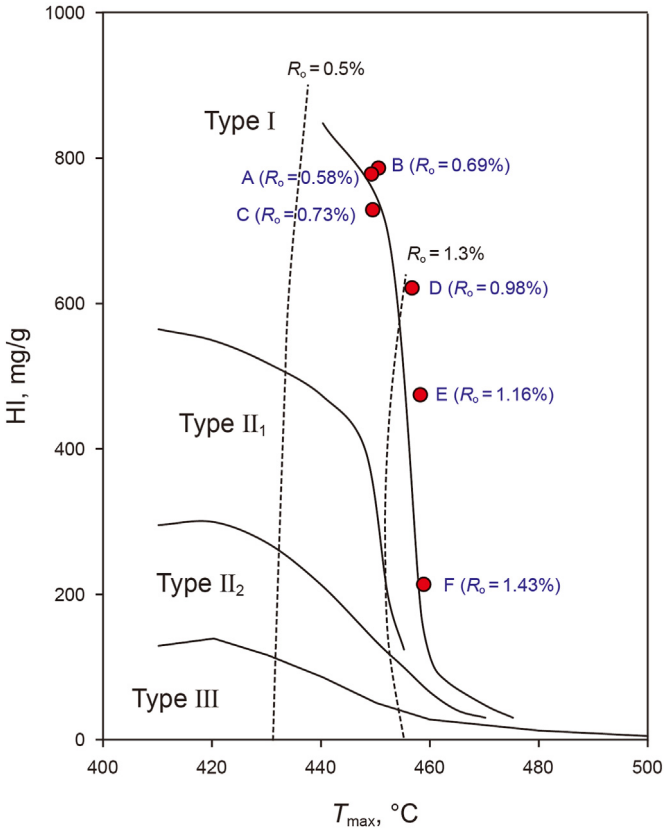

Fig. 2. Crossplot of T_{max} versus hydrogen index (HI) (according to Espitalié et al., 1984) with proposed kerogen types and maturity of the six samples.

3.2. Petrographic analysis of the OM

3.2.1. Low mature samples

At the low mature stages (R_o = 0.58%–0.69%), the primary macerals are alginite, bituminite and liptodetrinite. The precursors of alginite include unicellular, solitary, or colonial algae of planktonic and benthic origin. Alginite can be further divided into telalginite and lamalginite. Lamalginite is usually distinguished from telalginite by its thickness (< 0.005 mm), thickness/length ratio (< 0.5), and whether it has internal plant structure (Pickel et al., 2017). In this study, the size of alginite is generally < 5 μm in thickness and > 50 μm in lateral extent, the ratio of thickness to length of < 0.5 and no plant cell structure was observed in its interior (Fig. 3a-b, i-j). So, it is interpreted as lamalginite. Bituminite is the microbial degradation product of phytoplankton, zooplankton, and bacterial biomass (Kus et al., 2017; Pickel et al., 2017; Liu et al., 2020), it has no specific form. It can occur as irregular shape and elongate or fine laminations with mineral matrix. The length of it is 2 μm (Fig. 3e-f). Liptodetrinite is a maceral of the liptinite group consisting of extremely small particle, which composes of spores, pollen, particularly algae that have been chemical-microbiological decomposition (Pickel et al., 2017). The size is often only 2–3 μm in lateral extent with threadlike structures (Fig. 3b, j). In reflected white light, lamalginite is brown (Fig. 3a, i), and bituminite is almost black (Fig. 3e), while liptodetrinite cannot be identified. It is because the reflectance of liptodetrinite is < 0.1% in low maturity rocks (Pickel et al., 2017). In incident fluorescence illumination, lamalginite is yellow to orange and liptodetrinite is greenish yellow to orange (Fig. 3b, j). Bituminite do not fluoresce in the low mature stage (Fig. 3f).

Only minor amounts of the vitrinite and inertinite were found (Fig. 3c-d, g-h). The color of vitrinite is dark gray under reflected white light (Fig. 3c, g) and red-brown to black in fluorescence illumination (Fig. 3d, h), and its length ranges between 10 and 60 μm and the width is about 5 μm. Inertinite is greyish white to yellowish-white under reflected light (Fig. 3c) and weakly fluorescent (Fig. 3d), exists in irregular shapes, with 10 μm in length and 1 μm in width.

The SB occurs in the form of initial-oil solid bitumen (Fig. 3k-l), which is the product of the bitumen that is generated from primary

Table 1
Bulk geochemical parameters and dominant macerals type of samples from K_2qn_1 Formation.

Sample number	TOC, w.t.%	S_1, mg/g	S_2, mg/g	T_{max}, °C	S_1+S_2, mg/g	HI, mg/g	R_o	*PI*	Dominant macerals type
A	3.48	1.00	26.81	449	27.81	771	0.58%	0.036	Liptodetrinite and Lamalginite
B	3.82	2.06	29.63	450	31.69	775	0.69%	0.065	Liptodetrinite and Lamalginite
C	3.88	2.81	28.29	450	31.10	730	0.73%	0.090	Liptodetrinite and Lamalginite
D	5.13	4.97	31.52	457	36.49	615	0.98%	0.136	Solid bitumen
E	3.26	4.11	15.26	458	19.37	468	1.16%	0.212	Solid bitumen
F	3.58	3.55	7.38	460	10.93	206	1.43%	0.325	Solid bitumen and Pyrobitumen

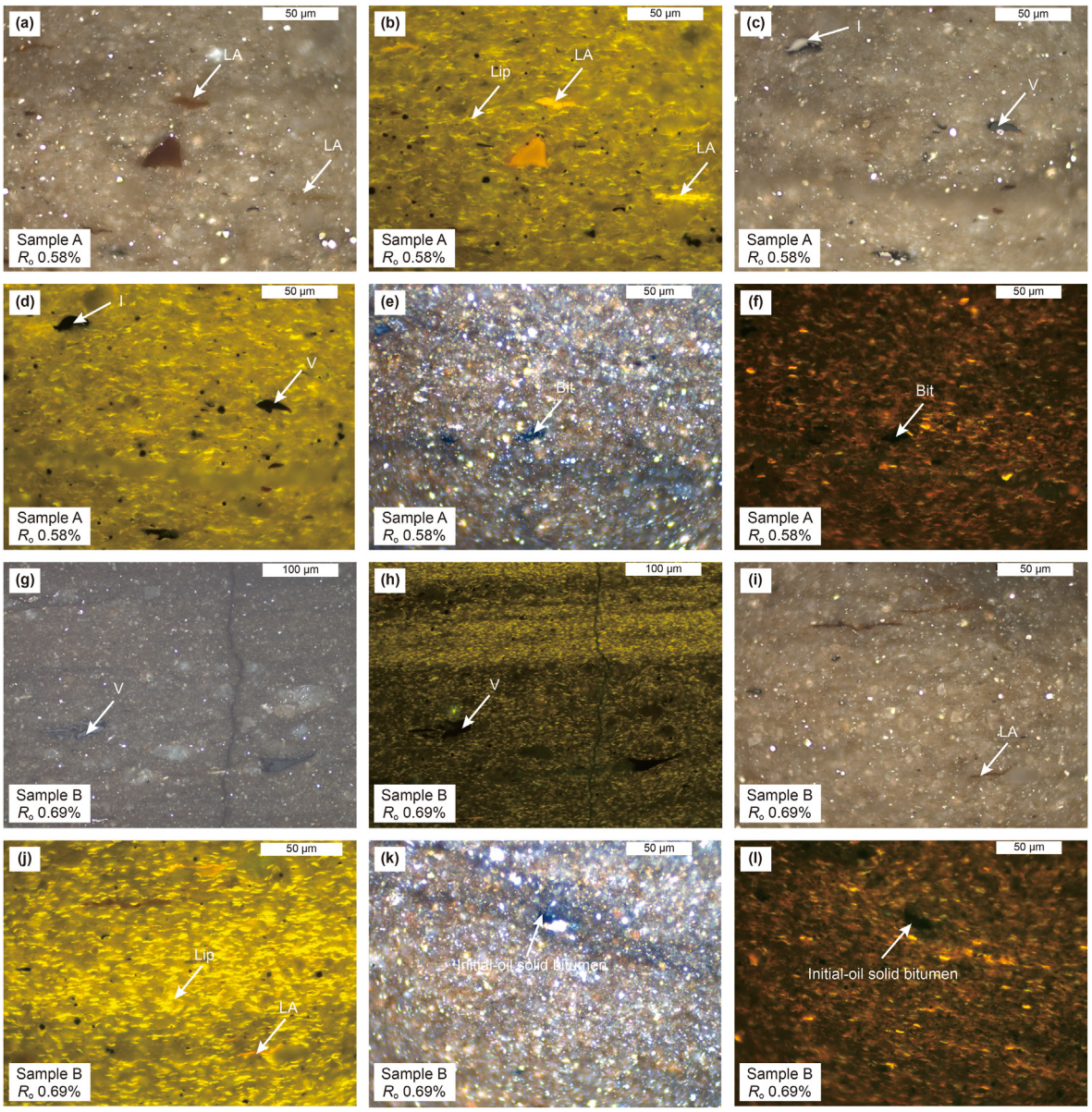

Fig. 3. Photomicrographs of macerals in reflected white light (a, c, e, g, i, k) and in fluorescence mode (b, d, f, h, j, l) using oil immersion objective. R_o ranges from 0.58% to 0.69%. LA: Lamalginite, Bit: Bituminite, Lip: Liptodetrinite, I: Inertinite, V: Vitrinite.

thermal cracking of kerogen (Sanei, 2020). The generated initial-oil solid bitumen shows dark black in the reflected light and no fluoresce (Fig. 3k-l), often occupying the place of precursor OM or migrate to pores and fractures in a short distance rather than long distance or regional migration.

3.2.2. Mature samples

At the early stages of oil generation (R_o = 0.73%), the fluorescence of lamalginite has altered from the original yellow to dull orange while the fluorescence of the liptodetrinite has changed to orange (Fig. 4a-b). Bituminite is still mixed with the mineral matrix and appears black under reflected white light (Fig. 4e). A small amount of SB is formed, with a length of 30 μm and a width of 5 μm (Fig. 4c-d). At the peak oil generation (R_o = 0.98%), the content of SB has increased significantly, and become the dominant organic component, but does not show any fluorescence (Fig. 4f-g). Only a few of liptodetrinites were observed, with dull orange fluorescence and a length of about 20 μm (Fig. 4g). At the late stages of oil generation, alginite, bitiminite and liptodetrinite were not observed and SB is still the principal organic constituent and distributed within the mineral matrix (Fig. 4j).

3.2.3. High mature samples

At higher thermal maturity stage (R_o = 1.43%), SB is the dominant OM filling the mineral interparticle pores (Fig. 4l). Alike lower maturity samples, vitrinite and inertinite were minor constituents of the OM and are distributed in fragmented discrete forms (Fig. 4c-d, h-i, k).

3.3. SEM observations

3.3.1. Organic pores

At the low mature stages (R_o = 0.58%–0.69%), OM is mostly elongated or linearly distributed along the minerals boundaries and

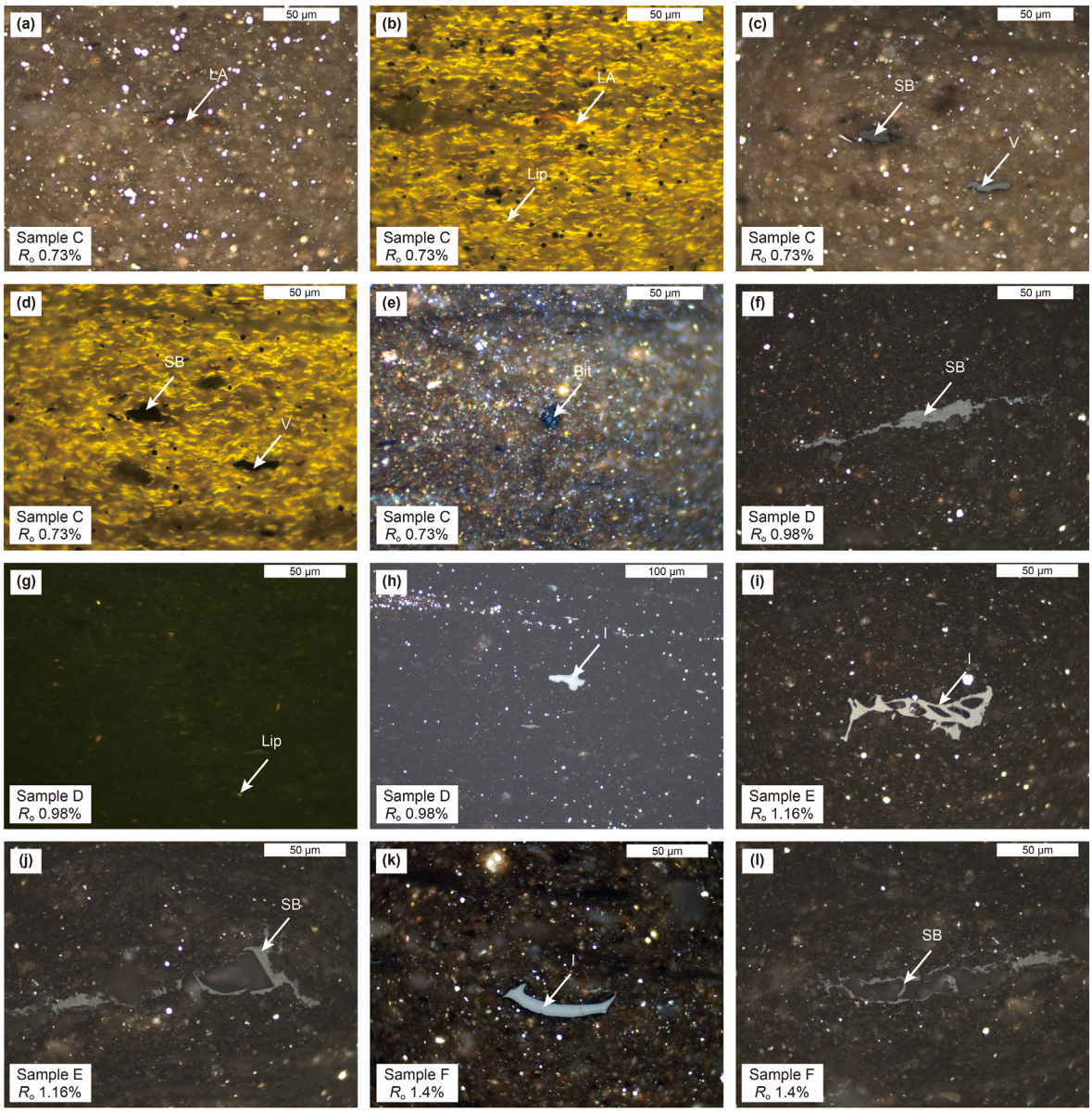

Fig. 4. Photomicrographs of macerals in reflected white light (a, c, e, f, h-l) and in fluorescence mode (b, d, g) using oil immersion objective. R_o ranges from 0.73% to 1.4%. LA: Lamalginite, Bit: Bituminite, Lip: Liptodetrinite, I: Inertinite, V: Vitrinite.

no primary pores were found (Fig. 5a, f). The surrounding mineral composition varies and can include quartz, clay minerals, carbonate, and pyrite. A small part of the OM exists in the mineral matrix as isolated forms, ranging from 10 to 20 μm in length and 3–5 μm in width, while organic pores were rarely found (Fig. 5b, e). OM-clay complexes show irregular shape, with length ranging between 2 and 30 μm (Fig. 5c-d, g-h). In these OM particles, isolated pores with irregular aggregated shapes at nanometer-scale were observed in the OM (Fig. 5d, h).

At the early oil generation stage (R_o = 0.73%), the OM shrinks and the cracks consistent with the shape of the OM appears at the edges (Fig. 5j, l). Furthermore, at the peak oil window (R_o = 0.98%), the existing forms of OM can be divided into two separate types: one is similar to what was observed in the isolated OM at the low thermal maturity, with a length of 25 μm and which is devoid of pores (Fig. 6e). While the other is the OM that is associated with clay minerals or quartz which contains bubble pores (Fig. 6b), with some of them being connected or fused together (Fig. 6c). The bubble pores occur in high abundance, and they can be up to several micrometers in size. The OM surrounded quartz grains, and micro-fractures are developed at the edges of the OM and quartz particles (Fig. 6a, d). At the late oil maturity stage (R_o = 1.17%), the pores developed in the OM that is associated with minerals are less abundant compared to those in the peak oil generation window, and the pores are filled by OM (Fig. 6f-g).

In the high-maturity sample (R_o = 1.43%), abundant spongy pores are evident in the OM and the diameter of the pores was found between 10 nm and 100 nm (Fig. 7a-b). Ultimately, a combination of OM with quartz as well as isolated OM are recognized, but they lack organic pores (Fig. 6h-i).

3.3.2. Inorganic pores

The development of organic pore network is influenced by surrounding inorganic minerals and diagenesis. Therefore, it is

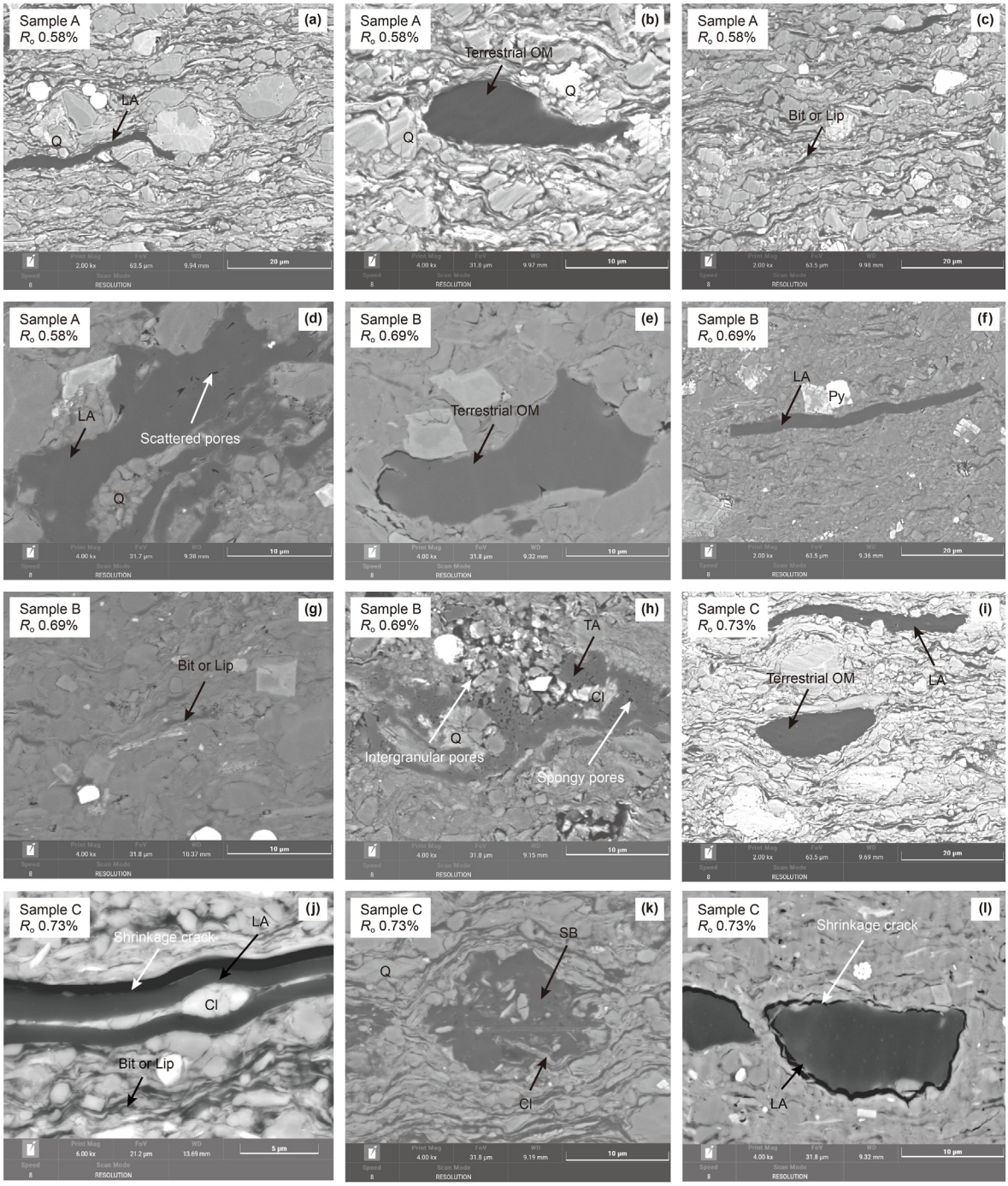

Fig. 5. SEM images showing types of OM and organic pores from low mature to the early oil window stage. Black arrows are OM types as well as mineral types and white arrows are organic pore types. The R_o of a-d SEM images is 0.58%, e-h is 0.69%, i-l is 0.73%. (a) Lamalginite without organic pores. (b) Terrestrial OM (inertinite or vitrinite) without organic pores. (c) Bituminite and liptodetrinite without organic pores (d) Scattered organic pores developed within alginite. (e) Terrestrial OM (inertinite or vitrinite) without organic pores. (f) SEM image of lamalginite. (g) SEM image of bituminite and liptodetrinite as organic streaks parallel to the bedding plane. (h) Spongy pores developed within alginite, which is the primary OM pores. (i) SEM image of lamalginite and Terrestrial OM. (j) SEM image of lamalginite, bituminite and liptodetrinite. Shrinkage crack, which is formed by the overall shrinkage of telalginite after hydrocarbon generation. (k) Clay minerals are coated with SB, which belong to migrated OM with no visible pores. (l) Shrinkage crack developed within lamalginite. LA: Lamalginite, Lip: Liptodetrinite, Bit: Bituminite, Terrestrial OM: Inertinite or vitrinite, SB: Solid bitumen, Q: Quartz, Py: Pyrite, Cl: Clay.

necessary to understand the development of inorganic pores at different stages. At the lower mature stages (R_o = 0.58%–0.69%), ductile components (clay mineral, OM) were strongly affected by mechanical compaction, such as clay minerals that were deformed in between layers to form interparticle pores (Fig. 8a). However, the stiffer minerals (e.g., quartz, pyrite) can strengthen the rock framework and reduce the influence of compaction on the pores (Fig. 8b). In addition, dispersed primary intraparticle pores can be observed at lower thermal mature stage that were measured in sizes from 20 nm to 300 nm (Fig. 8a). Moreover, at the oil generation window (R_o = 0.73%–1.16%), the interparticle pores of clay minerals have become abundant and the pore sizes are more than

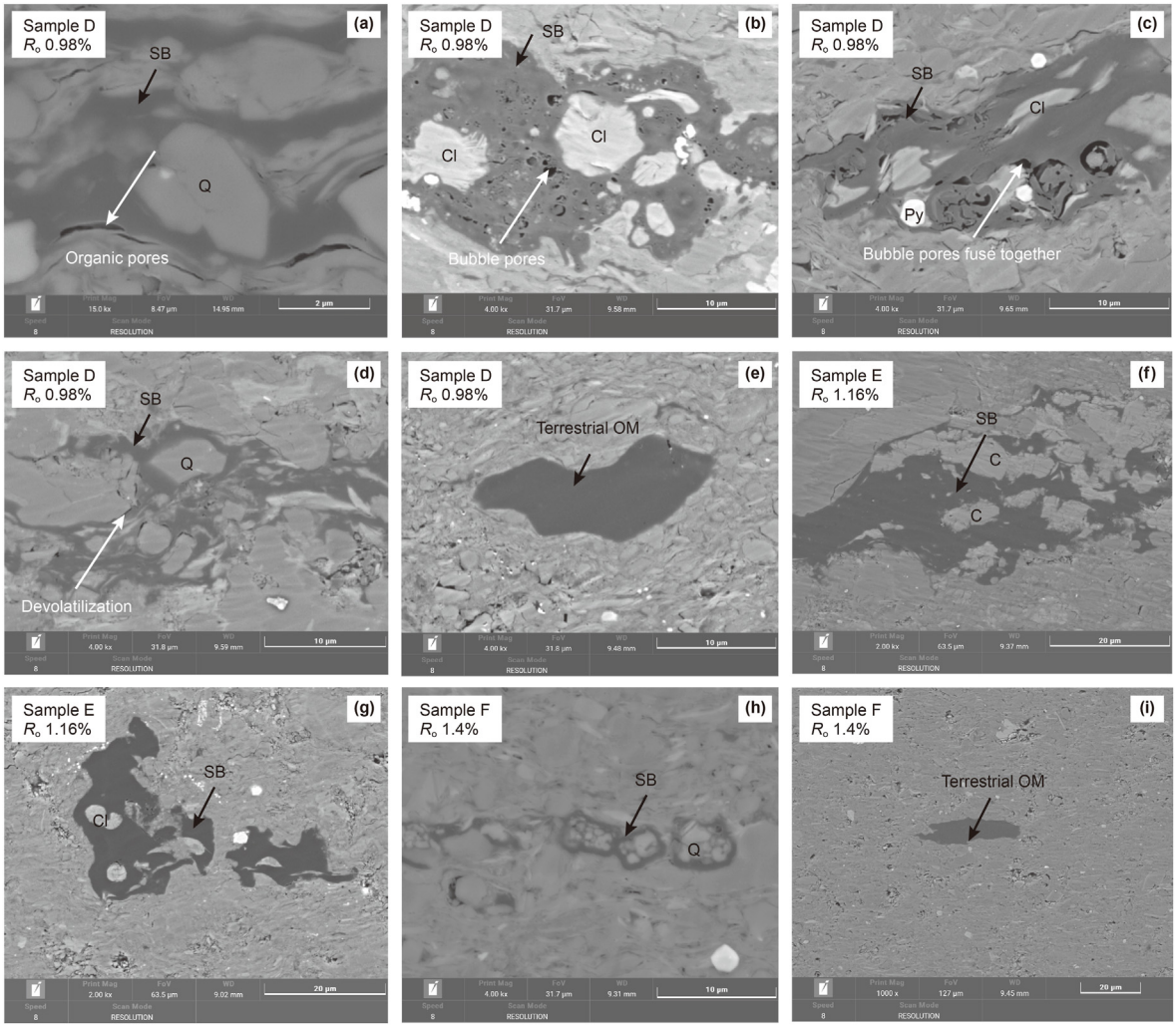

Fig. 6. SEM images showing types of OM and organic pores from the peak oil mature to high mature stage. Black arrows refer to OM types as well as mineral types and white arrows refer to organic pores. The R_o of a-e SEM images is 0.98%, f-g is 1.16%, h-i is 1.4%. (a) SEM images of secondary maceral types, SB. (b) Organic-clay complexes, abundant bubble pores in SB. (c) Organic-clay complexes, bubble pores developed within SB, some of the bubble pores are fused together. (d) Organic-quartz complex, quartz is enveloped with SB indicating quartz growth before bitumen emplacement, devolatilization cracks developed between SB and quartz. (e) Terrestrial OM (inertinite or vitrinite) without organic pores. (f) SB filled the pores between carbonate minerals. (g) SB is filled with authigenic minerals (h) Quartz is enveloped with SB indicating SB is migrated OM. (i) Terrestrial OM (inertinite or vitrinite) without organic pores. Terrestrial OM: Inertinite or vitrinite SB: Solid bitumen. Q: Quartz. Py: Pyrite. Cl: Clay. C: Carbonate.

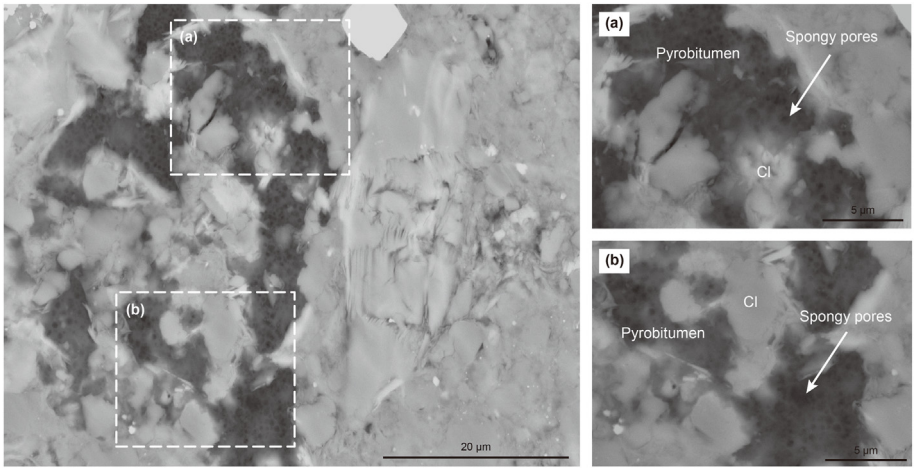

Fig. 7. SEM images showing spongy pores in pyrobitumen (sample E, R_o = 1.4%).

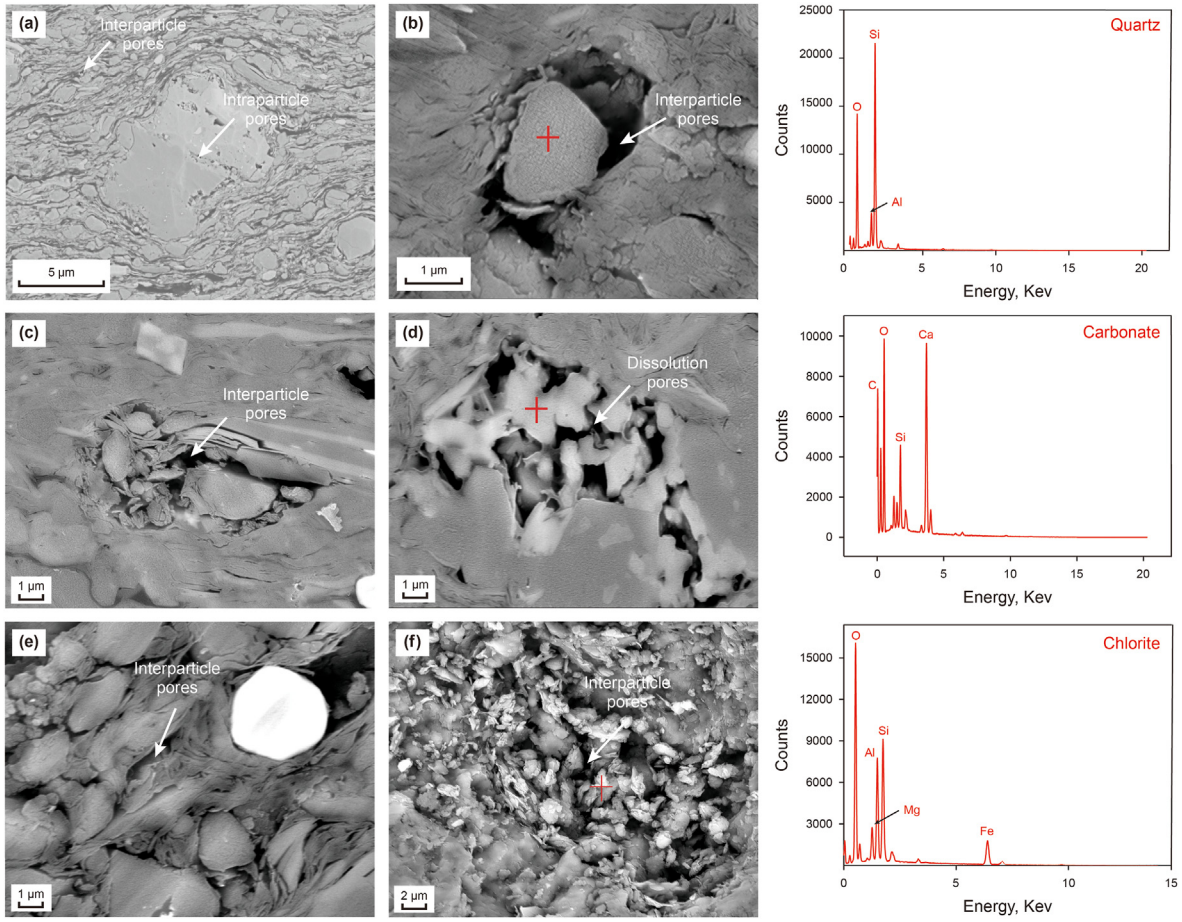

Fig. 8. SEM images showing inorganic pores from low mature to high mature stage. (a): interparticle pore and intraparticle pore (white arrow), sample A, R_o = 0.58%. (b) Quartz protects the interparticle pores (white arrow) by limiting the compaction, sample A, R_o = 0.58%. (c) Interparticle pores, sample C, R_o = 0.73%. (d) Dissolution pores in carbonate minerals, sample D, R_o = 0.98%. (e) Interparticle pores, sample E, R_o = 1.16%. (f) Interparticle pores in chlorite, sample F, R_o = 1.4%.

100 nm (Fig. 8c, e). Carbonate dissolution pores were also observed in this thermal maturity range (Fig. 8d). Finally, at higher maturity levels (R_o = 1.43%), interparticle pores in chlorite are the main type of inorganic pores, and can be up to several micrometers in size. (Fig. 8f).

3.4. The character of macerals identified by SEM

Three general forms of OM morphologies according to Ko et al. (2018) were identified in the Qingshankou Formation shale samples under the SEM as the pure OM, OM-mineral admixtures, and particulate OM while each is representing different maceral types (Fig. 9a).

In this regard, the pure OM corresponds to lamalginite from low to early oil maturity stage (R_o = 0.58%–0.72%), shows clearly defined boundary with the surrounding minerals. OM particles were generally elongated and parallel to the bedding under the influence of compaction (Fig. 9a, c-d). OM-mineral admixtures mainly correspond to bituminite and liptodetrinite from the low to early oil maturity stages (R_o = 0.58%–0.72%). It appears as a string shaped mixed with the mineral matrix under the SEM images and no sharp boundary with surrounding minerals (Fig. 5c, g, j). Furthermore, the lamalginite mixed with minerals are larger than the bituminite (Fig. 5d, h). Finally, particulate OM corresponds to terrigenous OM (vitrinite and inertinite), which can be found from low to high thermal maturity stage (Fig. 5b, e, i, Fig. 6e, i), with no specific shape and size, and rarely compacted (Fig. 9a and b).

4. Discussion

4.1. Evolution of macerals during thermal maturation

Based on our observations, the maceral types recognized in the SEM images of Figs. 5 and 6 are separated to better explain the changes in the OM composition during thermal maturation.

4.1.1. Evolution of primary macerals during thermal evolution

Thermal maturation of OM is a key process leading to the generation and expulsion of hydrocarbon in the subsurface (Kharaka, 1980). This being said, primary macerals will follow a different thermal evolution mode because they undergo various thermal catalysis and thermal pyrolysis during diagenesis due to mounting temperature and pressure (Tissot et al., 1974; Mastalerz and Bustin, 1993).

When R_o is less than 0.98%, liptodetrinite and lamalginite are the dominant OM and in higher concentrations, which indicates that the Cretaceous period in the Songliao Basin provided abundant nutrient during the process of seawater intrusion (Wang L. et al., 2022). This which could have caused phenomenon such as the algae bloom, and greatly improved the productivity of the lake basin (Stasiuk, 1993). Bituminite is generally derived from algal degradation products or bacterial precursors (Hackley et al., 2018),

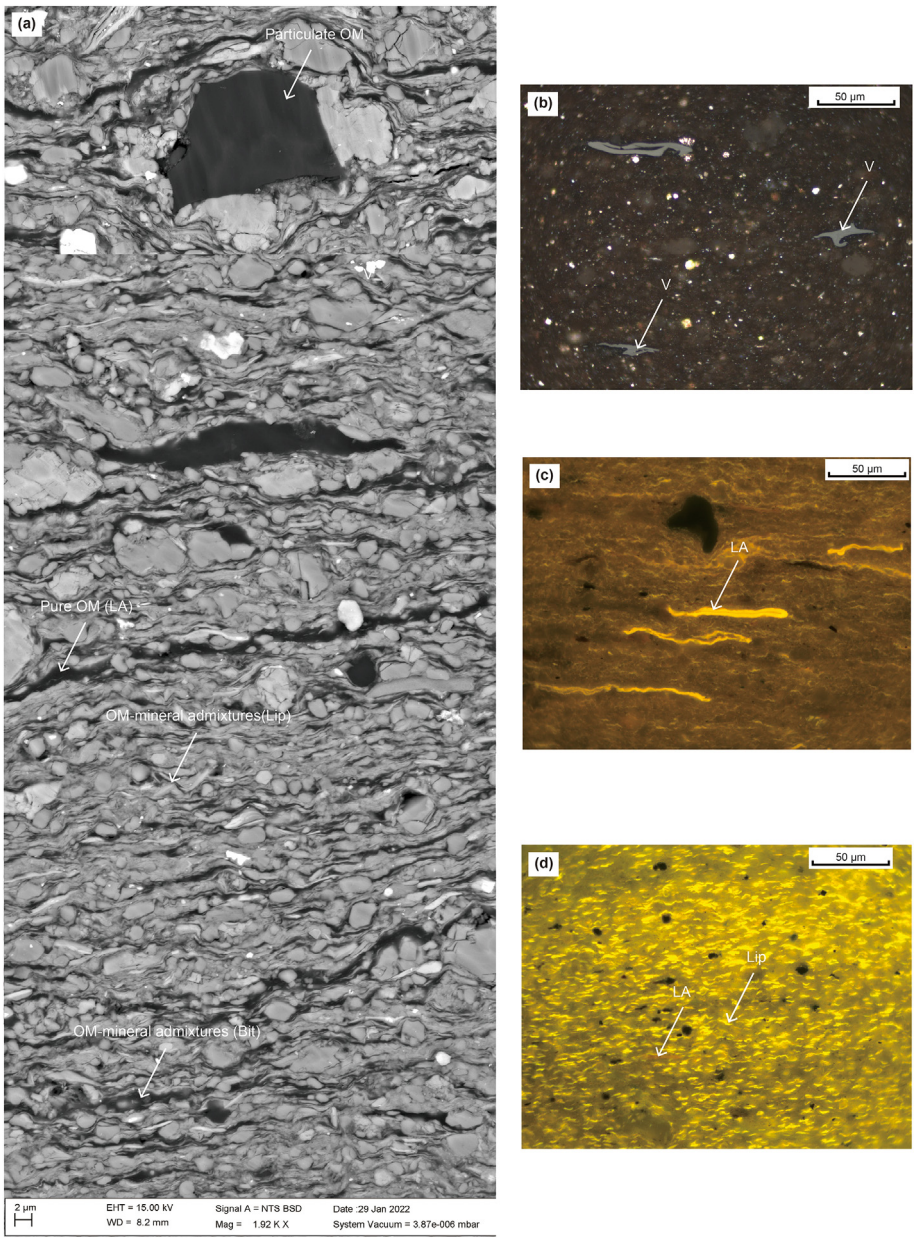

Fig. 9. Photomicrographs of the Qingshankou Formation shale sample identifying three distinct types of OM. (a) SEM image of three general forms of OM: (1) Pure OM. (2) OM-mineral admixture. (3) Particulate OM. Each is representing different maceral types. (b) Photomicrograph of vitrinite in reflected white light, which corresponds to particulate OM. (c) Photomicrograph of lamalginite in fluorescence, which corresponds to pure OM. (d) Photomicrograph of liptodetrinite in fluorescence, which corresponds to OM-mineral admixture. LA: Lamalginite, Lip: Liptodetrinite, Bit: bituminite, V: Vitrinite.

which are also widely present before the peak of hydrocarbon generation in the Qingshankou Formation, but less abundant than liptodetrinite and lamalginite. They began to transform into initial-oil solid bitumen at R_o 0.69% (Fig. 3k and l). Initial-oil solid bitumen is largely similar to Curiale (1986) genetic classification of "pre-oil solid bitumen", but not equivalent because the initial-oil solid bitumen forms exclusively within the oil window. At R_o 0.98%, the fluorescence disappeared, only a small amount of liptodetrinite were found and scattered sporadically, oil-prone kerogen transformed into SB and petroleum in large quantities. Lamalginite, liptodetrinite and bituminite are all oil-prone macerals, with high hydrogen content and aliphatic moieties, which can provide the original parent material for oil generation (Abarghani et al., 2020). Hence, they are almost entirely transformed during the peak of hydrocarbon generation. Additionally, compared to alginite and bituminite, terrigenous OM (vitrinite and inertinite) does not have any noticeable change during thermal maturation since it is more aromatic (Tissot et al., 1974).

4.1.2. Evolution of secondary macerals during thermal evolution

In the process of thermal evolution, it is easy to confuse the timing, origin and classification criteria of intermediate and secondary products, such as bitumen and SB. Bitumen is the secondary OM generated during catagenesis, which can be formed in two ways: (1) Early thermal cracking of oil-prone kerogen (Lewan, 1983). (2) Natural deasphalting and wax crystallization of liquid oil during the early oil and late oil -windows (Jacob, 1989). While SB is the secondary maceral, which was defined to distinguish it from

the primary macerals in the field of organic petrography (Mastalerz et al., 2018), formed due to natural deasphalting of crude oil, biodegradation, chemical dehydrogenation (oxidation), and thermal alteration of bitumen (Rogers et al., 1974; Machel, 2001; Synnott et al., 2016). According to the new genetic classification proposed by Sanei (2020), SB can be further divided into diagenetic solid bitumen, initial-oil solid bitumen, primary-oil solid bitumen, late-oil solid bitumen and pyrobitumen. Primary-oil solid bitumen and late-oil solid bitumen can be collectively referred to as post-oil bitumen.

In the studied shale samples, the initial-oil solid bitumen appeared at R_o 0.69% (Fig. 3k and l). According to the pyrosis results, the values of S_1 and S_2 at the R_o of 0.69% are higher than that at the R_o of 0.58%. It implies that initial-oil solid bitumen is an intermediate product of the transformation of kerogen into liquid petroleum, which is formed due to the breaking of weak (noncovalent) bonds (Ruble et al., 2020). Initial-oil solid bitumen is often associated with precursor oil prone kerogen and occupies its place (Sanei, 2020). Therefore, it is not easy to identify under SEM. Initial-oil solid bitumen primarily cracks to form oil, gas and post-oil SB (Fig. 10). At R_o of 0.73%, mineral crystals are surrounded by SB, specifying that the mineral growth happened before SB creation, and the SB later migrated to surround the mineral (Fig. 5k). Due to its high viscosity, it can only migrate a short distance, but lack a long distance, regional migration (Mastalerz et al., 2018). At R_o of 0.98%, SB has become the dominant constituent of the OM assemblage as solid bitumen replaces the original organic network of oil-prone kerogen. It is well documented that SB is the product of oil-prone kerogen degradation. Thus, SB formed at this maturity has lower viscosity than initial-oil solid bitumen and hence can migrate into farther and tighter pore structures (Jacob, 1989). Its flow path can easily be recognized. In this regard, the structural form the SB is usually consistent with the flow direction (Fig. 6d). In the high maturity stages, the liquid petroleum generated from the primary cracking undergoes a secondary cracking as the temperature increases, forming insoluble OM (pyrobitumen) and gas (Fig. 10). Post-oil bitumen also generates pyrobitumen and gas as the thermal evolution progresses. It indicates that both the secondary cracking of oil and the continuous thermal evolution of the remaining post-oil bitumen can lead to the formation of pyrobitumen and gas.

4.2. Evolution of organic pores during maturation

The evolution of organic pores is influenced by the composition and geochemistry of different maceral types and the effects of thermal alteration (Zhang et al., 2016). The size and shape of organic pores in different macerals are highly variable (Wood et al., 2015; Zhang et al., 2016; Misch et al., 2019). The distribution and properties of primary organic pores are controlled by the maceral types in the kerogen, while secondary organic pores are determined by the thermal maturity of the OM or migrated fluids (Mastalerz et al., 2018).

4.2.1. Organic pores evolution of primary macerals

Most oil-prone macerals do not host primary pores at the lower maturity stages (R_o = 0.58%–0.69%) (Fig. 11a1-a2). Based on the criteria of distinguishing deposited OM from migrated OM as proposed by Loucks and Reed (2014), OM occurring after cementation in the mineral pores provides the evidence of OM migration. However, our observations in this study show that oil-prone macerals have occupied the pore space in between adjacent rigid

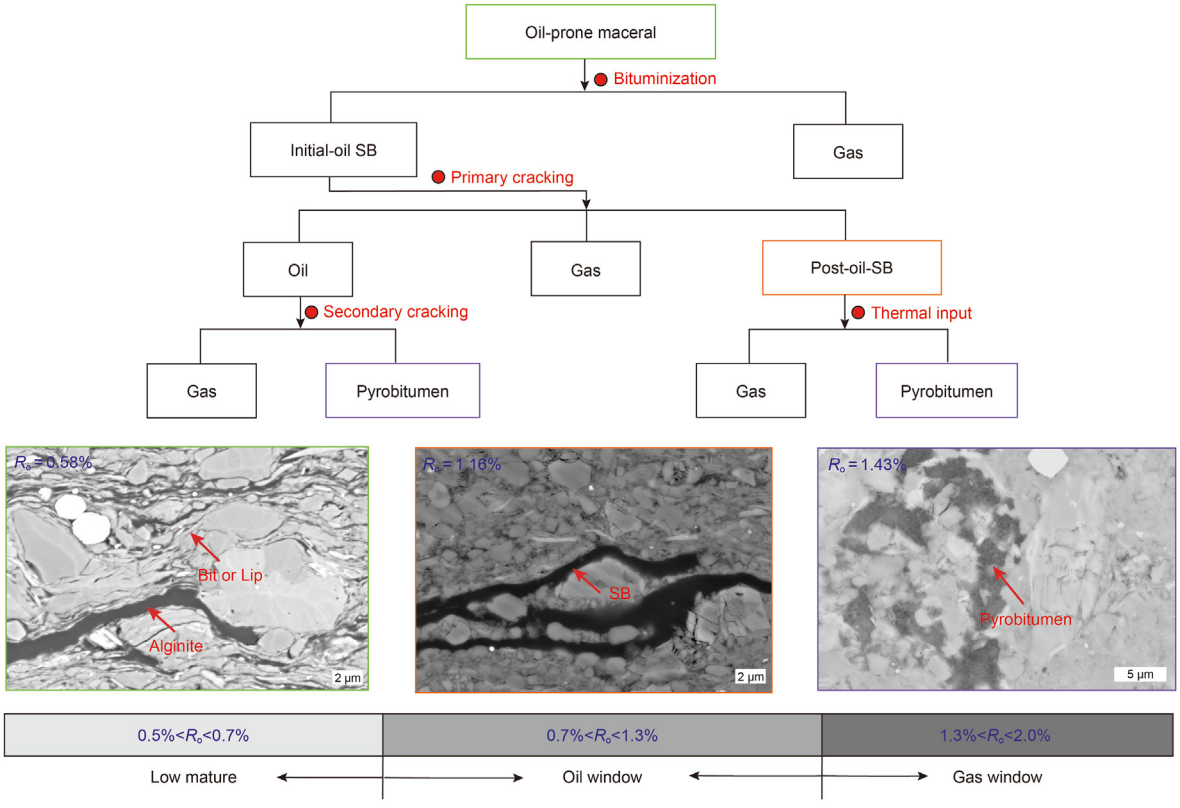

Fig. 10. Evolution of primary organic macerals and SB during hydrocarbon generation of the Qingshankou Formation shale. The rectangular border on the outside of the SEM image corresponds to the macerals in the evolution diagram. The SEM image in the green box corresponds to the oil-prone macerals (alginite, bituminite and liptodetrinite). The SEM image in the orange box corresponds to the SB. The SEM image in the purple box corresponds to the pyrobitumen. Bit: bituminite. SB: solid bitumen. Lip: Liptodetrinite.

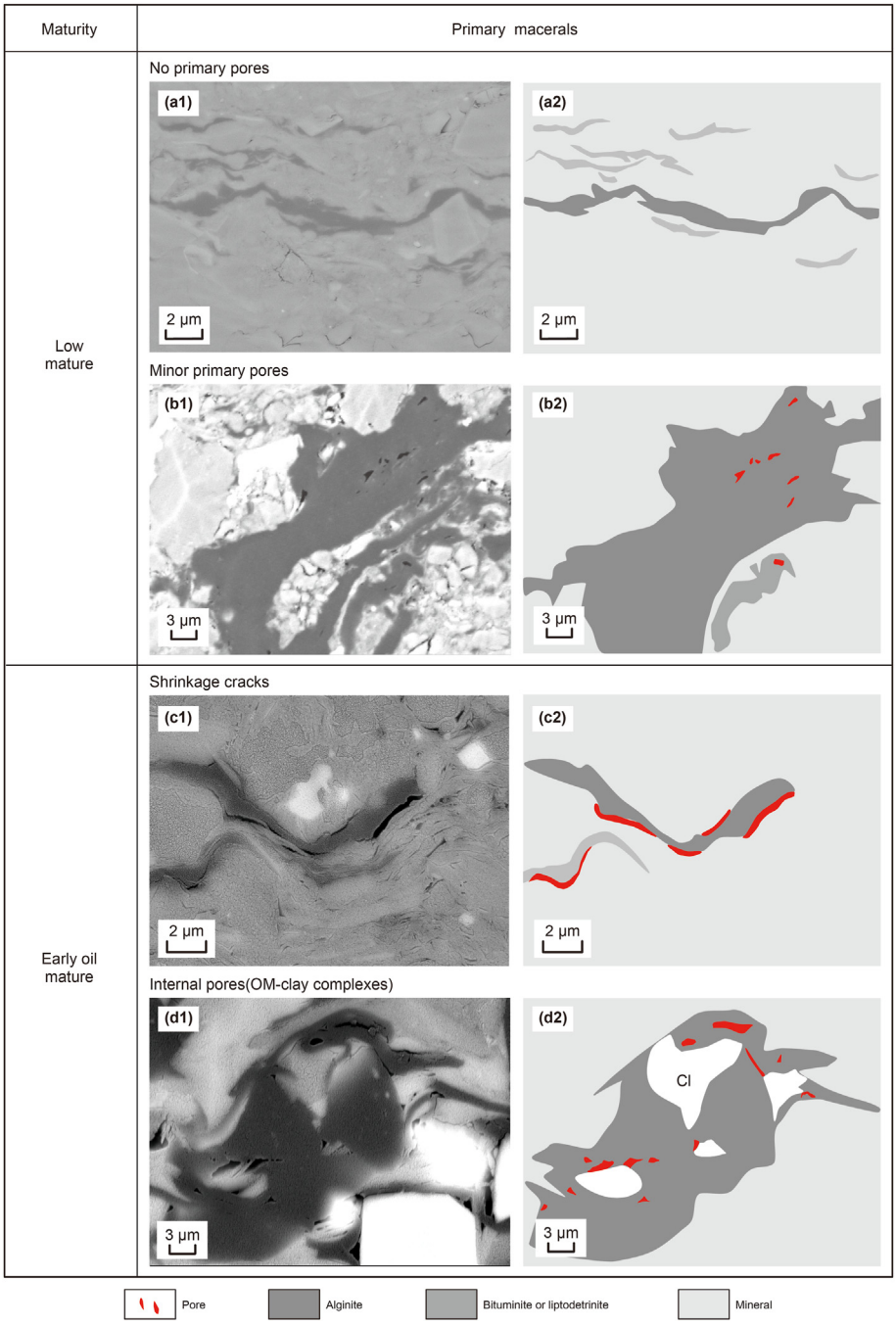

Fig. 11. The schematic for the organic pore evolution of the primary macerals in the Qingshankou Formation from the Songliao Basin.

mineral grains, which has left no pore space in minerals for later cementation (Fig. 5a, c). Oil-prone macerals are classified as deposited OM, while the associated primary organic pores are very limited (Fig. 11b1-b2). Some of these pores are isolated (Fig. 5d) while others are aggregated into a spongy shape (Fig. 5h). Previous studies have shown that scattered primary pores can be found in immature bituminite and alginite (Mastalerz et al., 2013; Löhr et al., 2015) and are aggregated together rather than exist as uniformly distributed spongy pores (Milliken et al., 2013). Here, that spongy pores are not limited to samples at the higher maturity stages, and pore aggregation is not a unique phenomenon that can only develop in pyrobitumen at the gas window. In the early oil generation window (R_o = 0.73%), there are two types of organic pores, shrinkage cracks and internal pores (Fig. 11c1-c2, d1-d2), which are formed when oil-prone macerals began to generate petroleum. Shrinkage cracks were found between the isolated alginite, bituminite and minerals (Fig. 5g, i), which is related to the morphology of OM and are produced during the decomposition reaction that is dominated by covalent bond cleavage (Ungerer, 1990). Internal pores were found on the alginite mixed with clay minerals, generated by the polycondensation reaction of chemical bonds (Ungerer, 1990). Compared to decomposition reaction, polycondensation reaction requires more energy to form organic internal pores, which indicates that internal pores are more difficult to form than shrinkage cracks. Moreover, it is possible that clay minerals present in the organic-clay mixture have a catalytic effect

on hydrocarbon generation (Rahman et al., 2017). Therefore, a large number of internal pores developed on the organic-clay complex in the early stage of oil generation while only shrinkage cracks developed within a single OM particle.

Finally, we did not identify any pores existing in vitrinite and inertinite at low maturity stages (Fig. 12a1-a2). This could be caused by the original plant cell structure degraded during the long distance of transportation of such macerals before deposition, leading to the primary cellular pores being destroyed. Besides, secondary pores were also not found from the oil window to higher mature stage in vitrinite and inertinite (Fig. 12b1-b2, c1-c2), which confirms they are highly stable, and their petroleum generation potential is limited during thermal evolution.

4.2.2. Organic pores evolution of secondary macerals

In-situ SB that transformed from alginite and bituminite begins to generate a large amount of petroleum at the thermal maturation of $R_o = 0.98\%$, leading to the generation of bubble pores (Fig. 13a1-a2). The formation of bubble pores is due to degassing during the transition from the oil window to the gas window (Katz and Arango, 2018). Meanwhile, some of the bubble pores can be united and form an irregular pore (Fig. 6c), which may be caused by structural changes in the kerogen (Reed et al., 2020). More abundant organic pores can be found in organic-clay mixtures rather than single OM at the peak of hydrocarbon generation (Fig. 13b1-b2). It further demonstrates the positive effect of clay minerals on hydrocarbon generation. This phenomenon takes place because the Qingshankou Formation is rich in smectite and detrital kaolinite in the early diagenetic stage (He et al., 2022). Affected by factors such as burial depth, compaction, temperature, and pressure, smectite dehydration gradually converts to mixed layer of smectite and illite. In the process of clay minerals transformation, interlayer water is expelled, which provides hydrogen ions for thermal evolution, thus promoting petroleum generation from OM (Tannenbaum et al., 1986). In addition, devolatilization cracks were found on the migrated SB (Fig. 13c1-c2), which are different from the shrinkage cracks observed at the early maturity stages as they are formed due to pressure release during the process of bringing the core to the surface rather than naturally (Loucks and Reed, 2014). If such cracks were naturally present in the subsurface, SB generated from neraby kerogen would have filled them. At the late oil generation window ($R_o = 1.16\%$), the abundance of secondary organic pores was less than that of at the peak oil generation since authigenic mineral cements (quartz, illite, chlorite) filled the organic pores (Fig. 13d1-d2). Smectite and kaolinite eventually disappeared to form authigenic minerals, such as chlorite and illite. In addition, the silica released during the conversion of smectite to illite causes authigenic quartz precipitation to occupy the pore space. Therefore, the

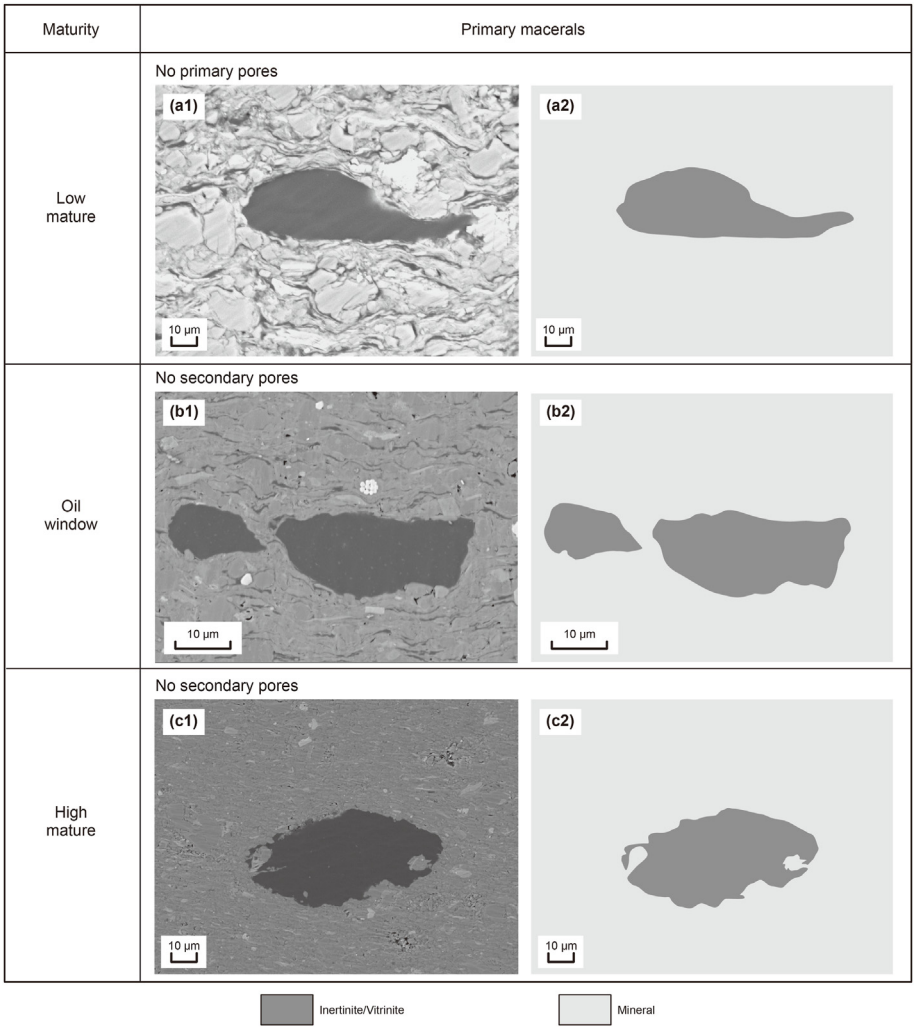

Fig. 12. The schematic for the organic pore evolution of the virtinite and inertinite in the Qingshankou Formation from the Songliao Basin.

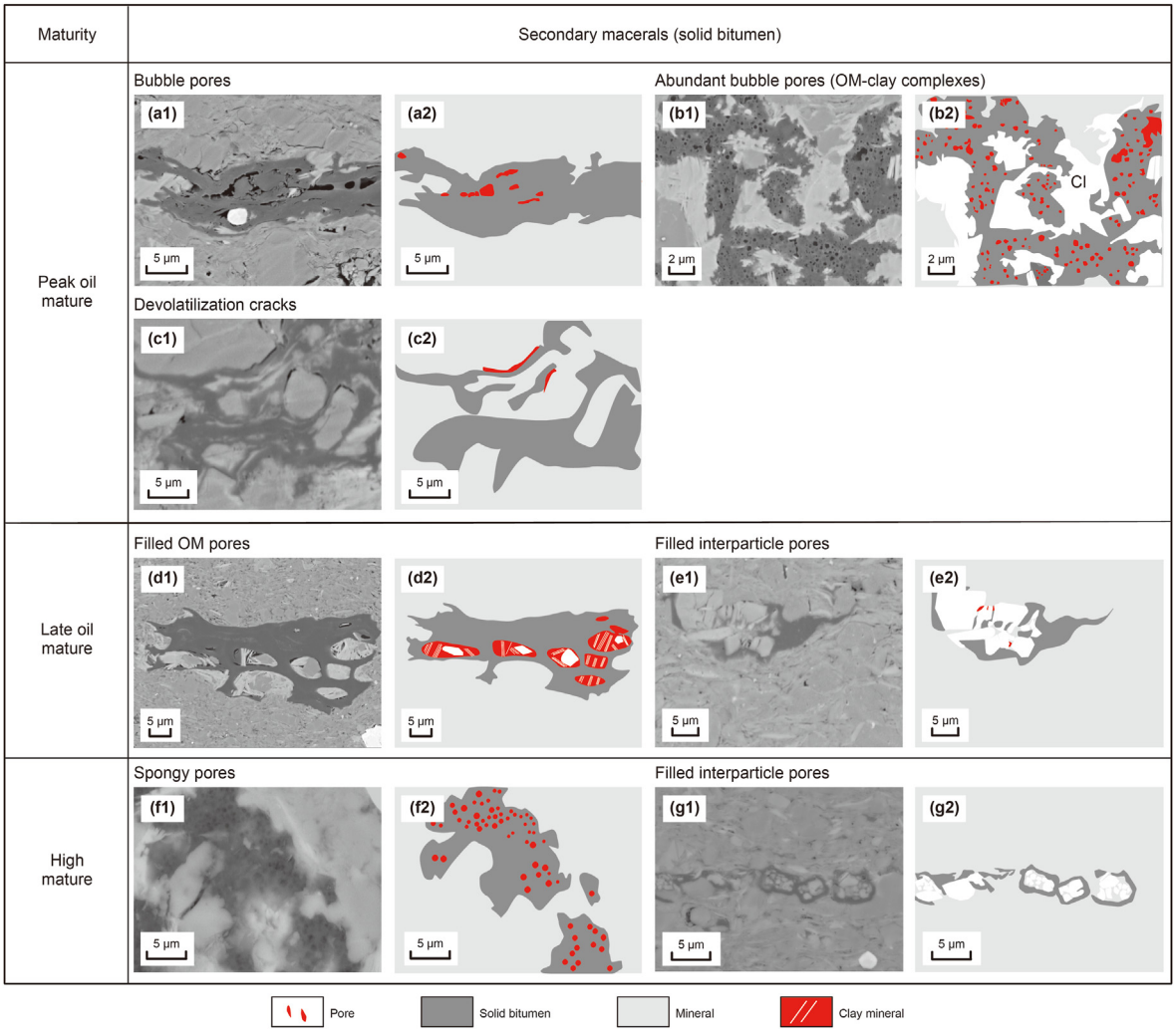

Fig. 13. The schematic for the organic pore evolution of secondary macerals (SB) in the Qingshankou Formation from the Songliao Basin.

organic-clay mixture developed abundant organic pores before the late oil maturity stage (Thyberg et al., 2010). In addition, interparticle mineral pores were filled by the migrated SB (Fig. 13e1-e2). Furthermore, the spongy pores exist in the pyrobitumen were found to be a significant feature at the higher maturity stages (Fig. 13f1-f2), where pyrobitumen formed by oil cracking continued to crack and generate small amounts of gas. Unlike the lower mature stage, the spongy pores that developed at the higher thermal maturity tend to grow and merge and to create more irregular shapes (Fig. 7). A general overview of the maturity stage that is reported when sponge pores are formed in different basins around the world (Dong et al., 2019; Reed et al., 2020; Lu et al., 2023), shows that such pores in the Qingshankou Formation, Songliao Basin, are generally created at later matuiriy stages than those of the Barnett and Woodford shales in North America. A potential explanation could be that when R_o is between 1.0% and 1.43% in the Songliao Basin, the existing overpressure system inhibits the cracking and gasification of crude oil (Carr, 1999), which extends the maturity for the preservation of oil compared to other basins. Ultimately, except for the sponge pores, organic pores found in SB are less abundant at higher mature stages, and the majority of interparticle pores were blocked by SB (Fig. 13g1-g2).

4.3. Comparision with other macerals and its related organic pores evolution model in different basins

Compared with maceral evolution and its related organic pores in other basins (Jarvie et al., 2007; Liu et al., 2017a, 2023b; Ko et al., 2016, 2018; Teng et al., 2022), it is found that there are similarities between oil-prone macerals evolution in different basins (Table 2). They are almost entirely converted to SB at the peak oil generation stage. While oil and SB further formed pyrobitumen and gas at high mature stage. In addition, it is observed that secondary pores are developed on pyrobitumen, whether marine shale or lacustrine shale (Bernard et al., 2012). Yet the transformation from gas-prone macerals (vitrinite and inertinite) to SB occurs significantly later (Mastalerz et al., 2018). Shrinkage crack is the unique pore type in the Qingshankou shale and there are mostly internal pores, such as bubble pores and spongy pores are more develped in marine shale. It is due to the type of primary macerals are different in marine and lacustrine shale. Lamalginite and liptodetrinite are the dominant primary macerals in the Qingshankou Formation, while the bituminite or Tasmanites cysts are the dominant primary macerals in marine shale (Liu et al., 2017a, 2019b). The lamalginite and liptodetrinite have a high hydrocarbon generation conversion rate and can form a large number of shrinkage cracks along the minerals. Variation in OM composition is the main factor for the difference in

Table 2
Comparision with other macerals and its related organic pores evolution model in different basins (LA: Lamalginite, Lip: Liptodetrinite, Bit: bituminite, T-OM: Terrestrial OM, SB: solid bitumen, Light gray represents the major maceral types and dark gray represents the major organic pores).

Stage / Basic Information	Lacustrine						Marine							
	Qingshankou Formation Songliao Basin Type I-Type II_1		Yanchang Formation (KQ section) Ordos Basin Type I		Yanchang Formation (DZ section) Ordos Basin Type III		New Albany Shale Illinois Basin Type II		Woodford Shale Permian Basin Algal-rich Type II		Barnett Shale Forth Worth Basin Type II		Wufeng-Longmaxi Shale Sichuan Basin Type I-Type II_1	
Immature-low mature ($R_o < 0.7\%$)	Lip LA and Bit Minor T-OM	Primary OM pores	/	/	/	/	Bit and Tas Minor T-OM	Cellular pores	Bit and Tas Minor T-OM	Primary OM pores	Bit Minor Tas and T-OM	Primary OM pores Convolu-ted OM pores	/	/
Early oil maturity ($R_o = 0.7\% - 0.85\%$)	Lip and Lam Initial-SB Minor T-OM	Shrinkage cracks Secondary pores	Bit and Al Minor T-OM	Cellu-lar pores	Vitrinite and inertinite	Cellular pores	Pre-oil bitumen Minor T-OM and SB	Cellular pores Secondary pores	Bit and Tas Minor T-OM	A few bubble pores	Bit Pre-oil bitumen Minor Tas and T-OM	Bubble pores	/	/
Peak oil maturity ($R_o = 0.85\% - 1.1\%$)	SB Minor T-OM	Bubble pores Devolatiliz-ation cracks	/	/	/	/	/	/	Post-oil bitumen	Bubble pores Moldic pores	Post-oil bitumen	Spongy pores	/	/
Late oil maturity ($R_o = 1.1\% - 1.4\%$)	SB Minor T-OM	Filled pores Devolatili-zation cracks	/	/	/	/	/	/	Post-oil bitumen	Moldic pores	Post-oil bitumen	Spongy pores		
High mature ($R_o = 1.4\% - 2.0\%$)	SB Pyro-Bitumen Minor T-OM	Spongy pores	/	/			SB Minor T-OM	Seconda-ry pores	Post-oil bitumen Pyro-bitumen	Spongy pores	Pyro-bitumen	Spongy pores	Pyro-bitumen and graptolites	Spongy pores

its pore characteristics between the Qingshankou shale and other typical marine shales. Therefore, in order to better characterize unconventional reservoirs in shale oil/gas systems, our study can provide a scientific example and guidance for understanding macerals types and associated pores evaluation during the thermal maturation.

5. Conclusions

(1) SB became the dominant OM constituent that transformed from the oil-prone macerals entirely at the peak oil window ($R_o = 0.98\%$), which replaces the original organic network of oil-prone kerogen. At higher maturity stage ($R_o > 1.43\%$), the secondary cracking of oil and the continuous thermal evolution of the remaining SB can lead to the formation of pyrobitumen and gas. Vitrinite and inertinite remained stable in all maturity stages because their low hydrocarbon generation potential.

(2) Primary organic pores were observed only in alginite at lower mature stages, and filled by SB subsequently. Due to oil and gas generation, alginite and bituminite shrunk and form shrinkage cracks at early oil window. At peak oil window, secondary bubble pores formed within the in-suit SB while devolatilization cracks developed in the migrated SB. From late oil window to higher maturity stages, secondary organic pores were less abundant than those at the peak oil generation, since they were filled by migrated SB. Spongy pores developed in the pyrobitumen at higher maturity stages ($R_o = 1.43\%$) are derived from the cracking of pyrobitumen into gas.

(3) From early to peak oil window, the organic-clay mixtures developed more organic pores than single OM, which is attributed to the clay minerals that have catalytic effect on petroleum generation. On the contrary, from late oil window and beyond, authigenic minerals, like chlorite and illite that evolved from smectite and kaolinite, will block and occupy the secondary organic pore spaces within the organic-clay mixtures.

Conflict of interest

No conflict of interest exits in the submission of this manuscript entitled “Maceral evolution of lacustrine shale and its effects on the development of organic pores during low mature to high mature stage”, and manuscript is approved by all authors for publication. I would like to declare on behalf of my co-authors that the work described was original research that has not been published previously, and not under consideration for publication elsewhere, in whole or in part. All the authors listed have approved the manuscript that is enclosed.

Acknowledgements

This work was financially supported by the National Natural Science Foundation of China (41972156) and the Natural Science Foundation of Heilongjiang Province (TD 2021D001).

References

American Society for Testing and Materials (ASTM), 2014. Standard test method for microscopical determination of the reflectance of vitrinite dispersed in sedimentary rocks: west Conshohocken, PA, ASTM International, Annual book of ASTM standards: petroleum products, lubricants, and fossil fuels; Gaseous fuels; coal and coke. sec 5, 823–830. https://doi.org/10.1520/D7708-11 v. 5.06, D7708-14. http://www.astm.org/Standards/D7708.htm.

Abarghani, A., Gentzis, T., Shokouhimehr, M., Liu, B., Ostadhassan, M., 2020. Chemical heterogeneity of organic matter at nanoscale by AFM-based IR spectroscopy. Fuel 261, 116454. https://doi.org/10.1016/j.fuel.2019.116454.

Bai, L.H., Liu, B., Du, Y.J., Wang, B.Y., Tian, S.S., Wang, L., Xue, Z.Q., 2022. Distribution

characteristics and oil mobility thresholds in lacustrine shale reservoir: insights from N2 adsorption experiments on samples prior to and following hydrocarbon extraction. Petrol. Sci. 19, 486–497. https://doi.org/10.1016/j.petsci.2021.10.018.

Bai, L., Liu, B., Yang, J., Tian, S., Wang, B., Huang, S., 2021. Differences in hydrocarbon composition of shale oils in different phase states from the Qingshankou Formation, Songliao Basin, as determined from fluorescence experiments. Front. Earth Sci. 15, 438–456. https://doi.org/10.1007/s11707-021-0915-8.

Bechtel, A., Jia, J., Strobl, S.A.I., Sachsenhofer, R.F., Liu, Z., Gratzer, R., Püttmann, W., 2012. Palaeoenvironmental conditions during deposition of the Upper Cretaceous oil shale sequences in the Songliao Basin (NE China): implications from geochemical analysis. Org. Geochem. 46, 76–95. https://doi.org/10.1016/j.orggeochem.2012.02.003.

Bernard, S., Wirth, R., Schreiber, A., Schulz, H.M., Horsfield, B., 2012. Formation of nanoporous pyrobitumen residues during maturation of the Barnett shale (fort worth basin). Int. J. Coal Geol. 103, 3–11. https://doi.org/10.1016/j.coal.2012.04.010.

Carr, A.D., 1999. A vitrinite reflectance kinetic model incorporating overpressure retardation. Mar. Petrol. Geol. 16, 355–377. https://doi.org/10.1016/S0264-8172(98)00075-0.

Curiale, J.A., 1986. Origin of solid bitumens, with emphasis on biological marker results. Org. Geochem. 10, 559–580. https://doi.org/10.1016/0146-6380(86)90054-9.

Curiale, J.A., Curtis, J.B., 2016. Organic geochemical applications to the exploration for source-rock reservoirs - a review. J. Unconv. Oil Gas Resour. 13, 1–31. https://doi.org/10.1016/j.juogr.2015.10.001.

Curtis, M.E., Cardott, B.J., Sondergeld, C.H., Rai, C.S., 2012. Development of organic porosity in the Woodford Shale with increasing thermal maturity. Int. J. Coal Geol. 103, 26–31. https://doi.org/10.1016/j.coal.2012.08.004.

Dong, T., Harris, N.B., Ayranci, K., Twemlow, C.E., Nassichuk, B.R., 2017. The impact of composition on pore throat size and permeability in high maturity shales: middle and Upper Devonian Horn River Group, northeastern British Columbia, Canada. Mar. Petrol. Geol. 81, 220–236. https://doi.org/10.1016/j.marpetgeo.2017.01.011.

Dong, T., Harris, N.B., McMillan, J.M., Twemlow, C.E., Nassichuk, B.R., Bish, D.L., 2019. A model for porosity evolution in shale reservoirs: an example from the upper devonian duvernay formation, western Canada sedimentary basin. Am. Assoc. Petrol. Geol. Bull. 103, 1017–1044. https://doi.org/10.1306/10261817272.

Espitalié, J., F. Marquis, and I. Barsony, 1984. Geochemical logging, in K. J. Voorhees, ed., Analytical pyrolysis: Techniques and applications:Boston, Butterworths, p.276–304, https://doi.org/10.1016/B978-0-408-01417-5.50013-5.

Furmann, A., Mastalerz, M., Bish, D., Schimmelmann, A., Pedersen, P.K., 2016. Porosity and pore size distribution in mudrocks from the belle fourche and second white specks formations in alberta, Canada. Am. Assoc. Petrol. Geol. Bull. 100, 1265–1288. https://doi.org/10.1306/02191615118.

Hackley, P.C., Valentine, B.J., Hatcherian, J.J., 2018. On the petrographic distinction of bituminite from solid bitumen in immature to early mature source rocks. Int. J. Coal Geol. 196, 232–245. https://doi.org/10.1016/j.coal.2018.06.004.

He, W., Liu, B., Sun, M., Wang, L., Zhang, J., Yasin, Q., Tian, S., Gao, S., Ukaomah, C.F., 2022. Pore types, genesis, and evolution model of lacustrine oil-prone shale: a case study of the Cretaceous Qingshankou Formation, Songliao Basin, NE China. Sci. Rep. 12, 17210. https://doi.org/10.1038/s41598-022-21154-y.

Huang, Y., Yang, G., Gu, J., Wang, P., Huang, Q., Feng, Z., Feng, L., 2013. Marine incursion events in the late cretaceous Songliao Basin: constraints from sulfur geochemistry records. Palaeogeogr. Palaeoclimatol. Palaeoecol. 385, 152–161. https://doi.org/10.1016/j.palaeo.2013.03.017.

International Committee for Coal Petrology (ICCP), 1998. The new vitrinite classification (ICCP System 1994). Fuel 77 (5), 349–358. https://doi.org/10.1016/S0016-2361(98)80024-0.

International Committee for Coal Petrology (ICCP), 2001. The new inertinite classifica- tion (ICCP System 1994). Fuel 80, 459–471. https://doi.org/10.1016/S0016-2361(00)00102-2.

Jacob, H., 1989. Classification, structure, genesis and practical importance of natural solid oil bitumen ("migrabitumen"). Int. J. Coal Geol. 11, 65–79. https://doi.org/10.1016/0166-5162(89)90113-4.

Jarvie, D.M., Hill, R.J., Ruble, T.E., Pollastro, R.M., 2007. Unconventional shale-gas systems: the Mississippian Barnett Shale of north-central Texas as one model for thermogenic shale-gas assessment. Am. Assoc. Petrol. Geol. Bull. 91, 475–499. https://doi.org/10.1306/12190606068.

Jarvie, D.M., 2012. Shale resource systems for oil and gas: shale-oil resource systems. In: Shale Reservoirs—Giant Resources for the 21st Century, vol. 97. American Association of Petroleum Geologists, pp. 89–119. https://doi.org/10.1306/13321447M973489.

Katz, B.J., Arango, I., 2018. Organic porosity: a geochemist's view of the current state of understanding. Org. Geochem. 123, 1–16. https://doi.org/10.1016/j.orggeochem.2018.05.015.

Kharaka, Y.K., 1980. Petroleum formation and occurrence. A new approach to oil and gas exploration. Earth Sci. Rev. 16, 372–373. https://doi.org/10.1016/0012-8252(80)90071-9.

Knapp, L.J., Ardakani, O.H., Uchida, S., Nanjo, T., Otomo, C., Hattori, T., 2020. The influence of rigid matrix minerals on organic porosity and pore size in shale reservoirs: Upper Devonian Duvernay Formation, Alberta, Canada. Int. J. Coal Geol. 227, 103525. https://doi.org/10.1016/j.coal.2020.103525.

Ko, L.T., Ruppel, S.C., Loucks, R.G., Hackley, P.C., Zhang, T., Shao, D., 2018. Pore-types and pore-network evolution in Upper Devonian-Lower Mississippian Woodford and Mississippian Barnett mudstones: insights from laboratory thermal maturation and organic petrology. Int. J. Coal Geol. 190, 3–28. https://doi.org/10.1016/j.coal.2017.10.001.

Ko, L.T., Loucks, R.G., Zhang, T., Ruppel, S.C., Shao, D., 2016. Pore and pore network evolution of Upper Cretaceous Boquillas (Eagle Ford–equivalent) mudrocks: results from gold tube pyrolysis experiments. Am. Assoc. Petrol. Geol. Bull. 100, 1693–1722. https://doi.org/10.1306/04151615092.

Kus, J., Araujo, C.V., Borrego, A.G., Flores, D., Hackley, P.C., Hámor-Vidó, M., Kalaitzidis, S., Kommeren, C.J., Kwiecińska, B., Mastalerz, M., Mendonça Filho, J.G., Menezes, T.R., Misz-Kennan, M., Nowak, G.J., Petersen, H.I., Rallakis, D., Suárez-Ruiz, I., Sýkorová, I., Životić, D., 2017. Identification of alginite and bituminite in rocks other than coal. 2006, 2009, and 2011 round robin exercises of the ICCP Identification of Dispersed Organic Matter Working Group. Int. J. Coal Geol. 178, 26–38. https://doi.org/10.1016/j.coal.2017.04.013.

Langford, F., Blanc-Valleron, M.-M., 1990. Interpreting Rock-Eval pyrolysis data using graphs of pyrolizable hydrocarbons vs. total organic carbon. Am. Assoc. Petrol. Geol. Bull. 74, 799–804. https://doi.org/10.1306/0C9B238F-1710-11D7-8645000102C1865D.

Lao, Y., Korth, J., Ellis, J., Crisp, P.T., 1989. Heterogeneous reactions of 1-pristene catalysed by clays under simulated geological conditions. Org. Geochem. 14, 375–379. https://doi.org/10.1016/0146-6380(89)90003-X.

Lewan, M.D., 1983. Effects of thermal maturation on stable organic carbon isotopes as determined by hydrous pyrolysis of Woodford Shale. Geochem. Cosmochim. Acta 47, 1471–1479. https://doi.org/10.1016/0016-7037(83)90306-X.

Liu, Z.J., Wang, D.P., Li, L., Liu, W.Z., Wang, P.J., Du, X.D., Yang, G., 1993. Sedimentary characteristics of the cretaceous in the Songliao Basin. Acta Geol. Sin. 6, 167–180. https://doi.org/10.1111/j.1755-6724.1993.mp6002005.x.

Liu, B., Lü, Y., Zhao, R., Tu, X., Guo, X., Shen, Y., 2012. Formation overpressure and shale oil enrichment in the shale system of lucaogou Formation, malang sag, santanghu basin, NW China. Petrol. Explor. Dev. 39, 744–750. https://doi.org/10.1016/S1876-3804(12)60099-8.

Liu, B., Schieber, J., Mastalerz, M., 2017a. Combined SEM and reflected light petrography of organic matter in the New Albany Shale (Devonian-Mississippian) in the Illinois Basin: a perspective on organic pore development with thermal maturation. Int. J. Coal Geol. 184, 57–72. https://doi.org/10.1016/j.coal.2017.11.002.

Liu, B., Bechtel, A., Sachsenhofer, R.F., Gross, D., Gratzer, R., Chen, X., 2017b. Depositional environment of oil shale within the second member of permian lucaogou Formation in the santanghu basin, northwest China. Int. J. Coal Geol. 175, 10–25. https://doi.org/10.1016/j.coal.2017.03.011.

Liu, B., Bechtel, A., Gross, D., Fu, X., Li, X., Sachsenhofer, R.F., 2018. Middle Permian environmental changes and shale oil potential evidenced by high-resolution organic petrology, geochemistry and mineral composition of the sediments in the Santanghu Basin, Northwest China. Int. J. Coal Geol. 185, 119–137. https://doi.org/10.1016/j.coal.2017.11.015.

Liu, K., Ostadhassan, M., Hackley, P.C., Gentzis, T., Zou, J., Yuan, Y., Carvajal-Ortiz, H., Rezaee, R., Bubach, B., 2019a. Experimental study on the impact of thermal maturity on shale microstructures using hydrous pyrolysis. Energy Fuels 33, 9702–9719. https://doi.org/10.1021/acs.energyfuels.9b02389.

Liu, B., Schieber, J., Mastalerz, M., 2019b. Petrographic and micro-FTIR study of organic matter in the Upper Devonian New Albany Shale during thermal maturation:Implications for kerogen transformation. In: Camp, W., Milliken, K., Taylor, K., Fishman, N., Hackley, P., Macquaker, J. (Eds.), Shale Diagenesis: Research Perspectives for Shale Hydrocarbon Reservoirs, Seals, and Source Rocks, vol. 120. AAPG Memoir, pp. 165–188. https://doi.org/10.1306/13672216M1213380.

Liu, B., Wang, H., Fu, X., Bai, Y., Bai, L., Jia, M., He, B., 2019c. Lithofacies and depositional setting of a highly prospective lacustrine shale oil succession from the Upper Cretaceous Qingshankou Formation in the Gulong sag, northern Songliao Basin, northeast China. Am. Assoc. Petrol. Geol. Bull. 103, 405–432. https://doi.org/10.1306/08031817416.

Liu, B., Mastalerz, M., Schieber, J., Teng, J., 2020. Association of uranium with macerals in marine black shales: insights from the upper devonian new Albany shale, Illinois basin. Int. J. Coal Geol. 217, 103351. https://doi.org/10.1016/j.coal.2019.103351.

Liu, B., Sun, J., Zhang, Y., He, J., Fu, X., Yang, L., Xing, J., Zhao, X., 2021. Reservoir space and enrichment model of shale oil in the first member of Cretaceous Qingshankou formation in the Changling sag, southern Songliao Basin: NE China. Petrol. Explor. Dev. 48, 608–624. https://doi.org/10.1016/S1876-3804(21)60049-6.

Liu, B., Mastalerz, M., Schieber, J., 2022a. SEM petrography of dispersed organic matter in black shales: a review. Earth Sci. Rev. 224, 103874. https://doi.org/10.1016/j.earscirev.2021.103874.

Liu, B., Wang, Y., Tian, S., Guo, Y., Wang, L., Yasin, Q., Yang, J., 2022b. Impact of thermal maturity on the diagenesis and porosity of lacustrine oil-prone shales: insights from natural shale samples with thermal maturation in the oil generation window. Int. J. Coal Geol. 261, 104079. https://doi.org/10.1016/j.coal.2022.104079.

Liu, B., Liu, L., Fu, J., Lin, T., He, J., Liu, X., Liu, Y., Fu, X., 2023a. The Songliao super basin in northeastern China. Am. Assoc. Petrol. Geol. Bull. 107, 1257–1297. https://doi.org/10.1306/02242321181.

Liu, B., Teng, J., Mastalerz, M., 2023b. Maceral control on the hydrocarbon generation potential of lacustrine shales: a case study of the chang 7 member of the triassic yanchang formation, ordos basin, north China. Energies 16 (2), 636. https://doi.org/10.3390/en16020636.

Löhr, S.C., Baruch, E.T., Hall, P.A., Kennedy, M.J., 2015. Is organic pore development in gas shales influenced by the primary porosity and structure of thermally immature organic matter? Org. Geochem. 87, 119–132. https://doi.org/10.1016/j.orggeochem.2015.07.010.

Loucks, R.G., Reed, R.M., Ruppel, S.C., Hammes, U., 2012. Spectrum of pore types and networks in mudrocks and a descriptive classification for matrix-related mudrock pores. Am. Assoc. Petrol. Geol. Bull. 96, 1071–1098. https://doi.org/10.1306/08171111061.

Loucks, R.G., Reed, R.M., 2014. Scanning-electron-microscope petrographic evidence for distinguishing organic-matter pores associated with depositional organic matter versus migrated organic matter in mudrocks. Gcags Transactions 3, 51–60.

Lu, C., Xiao, X., Gai, H., Feng, Y., Li, G., Meng, G., Gao, P., 2023. Nanopore structure characteristics and evolution of type III kerogen in marine-continental transitional shales from the Qinshui basin, northern China. Geoenergy Sci. Eng. 221, 211413. https://doi.org/10.1016/j.geoen.2022.211413.

Machel, H.G., 2001. Bacterial and thermochemical sulfate reduction in diagenetic settings - old and new insights. Sediment. Geol. 140, 143–175. https://doi.org/10.1016/S0037-0738(00)00176-7.

Mastalerz, M., Bustin, R.M., 1993. Variation in maceral chemistry within and between coals of varying rank: an electron microprobe and micro-Fourier transform infra-red investigation. J. Microsc. 171, 153–166. https://doi.org/10.1111/j.1365-2818.1993.tb03369.x.

Mastalerz, M., Drobniak, A., Stankiewicz, A.B., 2018. Origin, properties, and implications of solid bitumen in source-rock reservoirs: a review. Int. J. Coal Geol. 195, 14–36. https://doi.org/10.1016/j.coal.2018.05.013.

Mastalerz, M., Schimmelmann, A., Drobniak, A., Chen, Y., 2013. Porosity of Devonian and Mississippian New Albany Shale across a maturation gradient: insights from organic petrology', gas adsorption, and mercury intrusion. Am. Assoc. Petrol. Geol. Bull. 97, 1621–1643. https://doi.org/10.1306/04011312194.

Merey, S., Sinayuc, C., 2016. Analysis of carbon dioxide sequestration in shale gas reservoirs by using experimental adsorption data and adsorption models. J. Nat. Gas Sci. Eng. 36, 1087–1105. https://doi.org/10.1016/j.jngse.2016.02.052.

Milliken, K.L., Rudnicki, M., Awwiller, D.N., Zhang, T., 2013. Organic matter-hosted pore system, marcellus formation (devonian), Pennsylvania. Am. Assoc. Petrol. Geol. Bull. 97, 177–200. https://doi.org/10.1306/07231212048.

Misch, D., Gross, D., Hawranek, G., Horsfield, B., Klaver, J., Mendez-Martin, F., Urai, J.L., Vranjes-Wessely, S., Sachsenhofer, R.F., Schmatz, J., Li, J., Zou, C., 2019. Solid bitumen in shales: petrographic characteristics and implications for reservoir characterization. Int. J. Coal Geol. 205, 14–31. https://doi.org/10.1016/j.coal.2019.02.012.

Pickel, W., Kus, J., Flores, D., Kalaitzidis, S., Christanis, K., Cardott, B.J., Misz-Kennan, M., Rodrigues, S., Hentschel, A., Hamor-Vido, M., Crosdale, P., Wagner, N., 2017. Classification of liptinite – ICCP system 1994. Int. J. Coal Geol. 169, 40–61. https://doi.org/10.1016/j.coal.2016.11.004.

Pommer, M., Milliken, K., 2015. Pore types and pore-size distributions across thermal maturity, Eagle Ford Formation, southern Texas. Am. Assoc. Petrol. Geol. Bull. 99, 1713–1744. https://doi.org/10.1306/03051514151.

Rahman, H.M., Kennedy, M., Löhr, S., Dewhurst, D.N., 2017. Clay-organic association as a control on hydrocarbon generation in shale. Org. Geochem. 105, 42–55. https://doi.org/10.1016/j.orggeochem.2017.01.011.

Reed, R.M., Loucks, R.L., Ko, L.T., 2020. Scanning electron microscope petrographic differentiation among different types of pores associated with organic matter in mudrocks. Gulf Coast Association of Geological Societies 9, 17–27.

Rogers, M.A., McAlary, J.D., Bailey, N.J.L., 1974. Significance of reservoir bitumens to thermal-maturation studies, West Canada Basin. Am. Assoc. Petrol. Geol. Bull. 58, 1806–1824. https://doi.org/10.1306/83D919B6-16C7-11D7-8645000102C1865D.

Ruble, T.E., Hooghan, K., Bobby, Dorsey, W., Knowles, W.R., Laughrey, C.D., 2020. Pore-scale imaging of solid bitumens: insights for unconventional reservoir characterization. Mem. 120 mudstone diagenes. Res. Perspect. Shale hydrocarb. Reserv. Seals, source rocks. AAPG Memoir 120, 189–208. https://doi.org/10.1306/13672217m1213826.

Sanei, H., 2020. Genesis of solid bitumen. Sci. Rep. 10, 15595. https://doi.org/10.1038/s41598-020-72692-2.

Slatt, R.M., O'Brien, N.R., 2011. Pore types in the Barnett and Woodford gas shales: contribution to understanding gas storage and migration pathways in fine-grained rocks. Am. Assoc. Petrol. Geol. Bull. 95, 2017–2030. https://doi.org/10.1306/03301110145.

Stasiuk, L.D., 1993. Algal bloom episodes and the formation of bituminite and micrinite in hydrocarbon source rocks: evidence from the Devonian and Mississippian, northern Williston Basin, Canada. Int. J. Coal Geol. 24, 195–210. https://doi.org/10.1016/0166-5162(93)90010-8.

Synnott, D.P., Sanei, H., Pedersen, P.K., Dewing, K., Ardakani, O.H., 2016. The effect of bacterial degradation on bituminite reflectance. Int. J. Coal Geol. 162, 34–38. https://doi.org/10.1016/j.coal.2016.05.016.

Taylor, G.H., Teichmüller, M., Davis, A., Diessel, C.F.K., Littke, R., Robert, P., 1998. Organic Petrology. Gebrüder Borntraeger Stuttgart, Berlin, p. 704.

Tannenbaum, E., Huizinga, B.J., Kaplan, I.R., 1986. Role of minerals in thermal alteration of organic matter–II: a material balance. Am. Assoc. Petrol. Geol. Bull. 70, 1156–1165. https://doi.org/10.1306/94886a92-1704-11d7-8645000102c1865d.

Teng, J., Liu, B., Mastalerz, M., Schieber, J., 2022. Origin of organic matter and organic pores in the overmature ordovician-silurian wufeng-longmaxi shale of the Sichuan Basin, China. Int. J. Coal Geol. 253, 103970. https://doi.org/10.1016/j.coal.2022.103970.

Thyberg, B., Jahren, J., Winje, T., Bjørlykke, K., Faleide, J.I., Marcussen, Ø., 2010. Quartz cementation in Late Cretaceous mudstones, northern North Sea: changes in rock properties due to dissolution of smectite and precipitation of micro-quartz crystals. Mar. Petrol. Geol. 27, 1752–1764. https://doi.org/10.1016/j.marpetgeo.2009.07.005.

Tissot, B., Durand, B., Espitalié, J., Combaz, A., 1974. Influence of nature and diagenesis of OM in formation of petroleum. Am. Assoc. Petrol. Geol. Bull. 58, 499–506. https://doi.org/10.1306/83D91425-16C7-11D7-8645000102C1865D.

Ungerer, P., 1990. State of the art of research in kinetic modelling of oil formation and expulsion. Org. Geochem. 16, 1–25. https://doi.org/10.1016/0146-6380(90)90022-R.

Wang, B., Liu, B., Yang, J., Bai, L., Li, S., 2022. Compatibility characteristics of fracturing fluid and shale oil reservoir: a case study of the first member of Qingshankou Formation, northern Songliao Basin, Northeast China. J. Pet. Sci. Eng. 211, 110161. https://doi.org/10.1016/j.petrol.2022.110161.

Wang, L., Zhou, H.Y., Shang, F., Zhou, X.X., 2022. Element geochemical characteristics of black shale and paleo-sedimentary environmental restoration of Qingshankou Formation of the Cretaceous in the northern Songliao Basin. Geological Science 2022, 156–171. https://doi.org/10.12017/dzkx.2022.010.

Wood, J.M., Sanei, H., Curtis, M.E., Clarkson, C.R., 2015. Solid bitumen as a determinant of reservoir quality in an unconventional tight gas siltstone play. Int. J. Coal Geol. 150–151, 287–295. https://doi.org/10.1016/j.coal.2015.03.015.

Zhang, H., Zhu, Y., Wang, Y., Kang, W., Chen, S., 2016. Comparison of organic matter occurrence and organic nanopore structure within marine and terrestrial shale. J. Nat. Gas Sci. Eng. 32, 356–363. https://doi.org/10.1016/j.jngse.2016.04.040.

Zhang, P., Misch, D., Hu, F., Kostoglou, N., Sachsenhofer, R.F., Liu, Z., Meng, Q., Bechtel, A., 2021. Porosity evolution in organic matter-rich shales (Qingshankou Fm.; Songliao Basin, NE China): implications for shale oil retention. Mar. Petrol. Geol. 130, 105139. https://doi.org/10.1016/j.marpetgeo.2021.105139.

Zhou, J., Liu, B., Shao, M., Yin, C., Jiang, Y., Song, Y., 2022. Lithologic classification of pyroclastic rocks: a case study for the third member of the Huoshiling Formation, Dehui fault depression, Songliao Basin, NE China. J. Pet. Sci. Eng. 214, 110456. https://doi.org/10.1016/j.petrol.2022.110456.